Microchemical Journal 224 (2026) 117712

Contents lists available at ScienceDirect

Microchemical Journal

journal homepage: www.elsevier.com/locate/microc

Supramolecular β-cyclodextrin porous framework for selective extraction of diclofenac from environmental waters

Amelie Huber [a], Soumya Rajpal [a], Dionysis Adamou [b], Panayiota Demosthenous [b], Buse Parlak [a,c], Selis Onel [c], Boris Mizaikoff [a,*], Sherman Lesly Zambou Jiokeng [a,*]

[a] Institute of Analytical and Bioanalytical Chemistry, Ulm University, 89081 Ulm, Germany
[b] CY.R.I.C Cyprus Research and Innovation Center Ltd., 2643 Nicosia, Cyprus
[c] Hacettepe University, Chemical Engineering Department, Ankara 06800, Turkey

ARTICLE INFO

Keywords:
Diclofenac
Solid-phase extraction
Enrichment factor
Porous organic polymers
Box-Behnken design

ABSTRACT

Diclofenac (DF), a widely used non-steroidal anti-inflammatory drug, is frequently detected in environmental waters at ng/L to μg/L levels, requiring sensitive, selective, and affordable analytical methods for routine monitoring. Here, we developed and validated a supramolecular β-cyclodextrin-based porous organic polymer (POP) as a high-performance solid-phase extraction (SPE) sorbent for DF preconcentration from aqueous samples prior to UV–Vis analysis. The POP, synthesized from (2-hydroxypropyl)-β-cyclodextrin acrylate, was characterized by FTIR, FT-Raman, XRD, TGA, N_2 sorption, SEM, and ζ-potential measurements, confirming its porous, thermally stable structure, β-cyclodextrin-rich network, and inclusion complex formation. SPE parameters affecting extraction efficiency (EE) and enrichment factor (EF), including eluent type and volume, flow rates, sorbent mass, and conditioning pH, were optimized using one-factor-at-a-time studies and Box-Behnken design. The method exhibited linearity over 0.1–10 mg/L (method limit of detection: 18.0 ± 0.4 μg/L; method limit of quantification: 59.9 ± 1.2 μg/L). Field emulation experiments at 1500 ng/L DF in 1 L samples demonstrated EF values of 647 ± 159 (ultrapure water) and 549 ± 26.4 (real seawater), with recoveries of 64.7 ± 15.9% and 54.9 ± 2.6%, respectively. Compared to conventional C18 cartridges, the POP provided enhanced EE (98.75 ± 1.75%) and EF (373 ± 15 a.u.), highlighting its remarkable preconcentration capability. Molecular dynamics simulations revealed multi-point electrostatic and halogen-bonding interactions driving DF selectivity, while FT-Raman analysis of the POP-DF after sample loading confirmed the formation of an inclusion complex between the solid sorbent and the analyte. The results demonstrate the potential of β-cyclodextrin-functionalized POPs as efficient sorbents for preconcentration in trace-level pharmaceutical analysis of complex aqueous matrices.

1. Introduction

An emerging class of environmental pollutants is based on active pharmaceutical ingredients (APIs), as well as personal care products (PPCPs), especially if these chemicals are persistent and clean-up strategies by wastewater treatment plants are inefficient [1,2]. Even at low concentrations, these organic contaminants cause adverse effects on biota [3,4]. Diclofenac (DF), a substance belonging to a subclass called non-steroidal anti-inflammatory drugs (NSAIDs), is a therapeutic drug frequently used in, e.g., the treatment of osteoarthritis, rheumatoid arthritis, and sports injuries [5–9]. Contamination within a ng/L to μg/L concentration range across different environmental matrices, such as soil, bodies of water, drinking water, and in- and effluents of wastewater treatment plants (1–10 μg/L), has been reported [10–13]. Long-term effects of DF contamination include, e.g., developmental malfunctions, organ damage, and general impairment within aquatic wildlife [14–17]. The severity of the pollution and its related effects led the European Union to the addition of DF to the first watch list of emerging pollutants in 2013 [18]. The trace level detection and quantification of DF in environmental samples is currently employed by using chromatographic analytical techniques, such as gas chromatography mass spectrometry (GC/MS) [19,20], high-performance liquid chromatography (HPLC) [21], HPLC coupled to mass spectrometry (HPLC/MS) [22], liquid chromatography coupled to MS (LC/MS) [23], as well as MS [24], UV–Vis spectrophotometry [25], fluorimetry [26,27], and electrochemistry [28,29]. For quantification, sample pretreatment for effective

* Corresponding authors.
E-mail addresses: boris.mizaikoff@uni-ulm.de (B. Mizaikoff), sherman.jiokeng-zambou@uni-ulm.de (S.L.Z. Jiokeng).

https://doi.org/10.1016/j.microc.2026.117712
Received 2 January 2026; Received in revised form 4 March 2026; Accepted 13 March 2026
Available online 16 March 2026

separation and purification of complex real-world samples is often required, such as solid-phase extraction (SPE) [30,31]. SPE enables fast and reliable sample clean-up by removing matrix interferences, while enriching the isolated analyte for improved detection and quantification in subsequent analysis techniques [32]. For efficient preconcentration of any analyte from a given matrix the properties of the solid, as well as of the liquid phase, should be considered carefully to guarantee efficient removal and to avoid co-elution of interfering species from the sample. By implementing of porous sorbents bearing host-guest binding sites that are selective for the overall shape, size, and chemical structure of the targeted analyte, the extraction efficiency (EE) of an SPE set-up is improved [33].

Porous organic polymers (POPs) are prepared in a bottom-up approach by reacting purely organic monomers with suitable cross-linkers to form macromolecular networks that only contain light elements, such as carbon, hydrogen, boron, nitrogen, or oxygen [34–36]. In general, POPs are described as (highly) cross-linked structures capable of acting as host frameworks for guest molecules, often incorporating tailored binding sites for selective recognition [34–37]. POPs offer adjustable pore sizes and distributions, along with (hierarchical) porosity, high specific surface areas, and tunable chemical composition and structure, enabling the incorporation of functional groups tailored to specific analyte binding, either during synthesis or through post-functionalization [34,35,38]. Due to their polymeric matrix, POPs typically exhibit good mechanical stability and structural versatility, enabling their integration into membranes, fibers, and monoliths [35]. Given these characteristics, POPs are often applied in separation science of gas and liquid phases, water purification, molecular recognition, electrochemical energy storage, CO_2 capture, biomedical applications, and (heterogeneous) catalysis [35,37]. Their potential in SPE methods has been demonstrated for pollutant removal and sample pretreatment prior to sensing applications of environmental samples [35,38]. For example, Guo et al. [38] developed a triazine-triphenylphosphine-based POP as a sorbent for the selective SPE of nitroimidazoles from honey and water, showcasing its effectiveness in complex matrices with efficient pollutant recovery and enrichment. Incorporating supramolecular structures as monomeric units into POPs enables enhanced analyte separation by introducing well-defined nanocavities that serve as active binding sites. POPs are described as hierarchically porous, due to the presence of nanocavities and mesopores created by the polymerization technique used. A frequently used subclass of such supramolecular units are macrocycles, which act as host molecules for various guest species through reversible non-covalent interactions [38,39]. Herein, special attention is given to cyclodextrins (CDs), which are truncated cone-shaped cyclic oligosaccharides containing a hydrophilic exterior and a hydrophobic cavity. The size of the cavity depends on the amount of (α − 1,4)-linked D-glucopyranose units. This allows for selective host-guest interactions with hydrophobic analytes of suitable molecular size that fit into the cavity [40,41]. Their primary and secondary hydroxyl groups can be used for further functionalization, thus enabling modification to adjust solubility and binding properties, allowing integration into POPs via polymerization [33,39]. β-CD is composed of seven glucopyranose units, leading to an inner rim diameter at the secondary side of 6.0–7.8 Å, which is particularly suited for forming stable host-guest inclusion complexes with a range of hydrophobic pharmaceuticals, including DF [33,42]. The formation is facilitated by enthalpy-driven non-covalent host-guest interactions, including Van der Waals forces, hydrophobic interactions, and hydrogen bonds, with association constants typically ranging from 10^3 to 10^5 M^{-1} [43–45]. They are typically formed in a 1:1 stoichiometry, although higher-order complexes can also occur [40,42,46].

Since SPE performance depends on multiple interacting parameters, such as eluent type and volume, flow rates, sorbent amount, pH, ionic strength, type of washing solvent, and column dimensions, methodical optimization of the SPE process tailored to the specific analytical response is crucial. For efficient tailoring, the design of experiments (DoE) approach is preferred over the typical one-factor-at-a-time (OFAT) method, as DoE considers interdependencies of different parameters simultaneously [47]. The OFAT approach does not account for parameter interactions and requires a large number of experiments, resulting in extended research time and increased material consumption [48]. The response surface methodology (RSM) is an important subject in the statistics of DoE, aiming to assess the relative importance of several influential factors and to ultimately yield the best operating conditions by optimization of a set response [49]. It employs mathematical and statistical methods to model and analyze problems in which the response of interest is affected by multiple variables. The main objective of this study is to develop a SPE method that selectively extracts and enriches DF from aqueous samples, enabling environmentally relevant concentrations in the ng/L to μg/L range to be transferred into the validated UV–Vis calibration range for reliable detection and quantification. To address the challenges of detecting DF in complex environmental samples, a novel POP was designed by incorporating β-CD derivatives to provide host-guest binding sites. In contrast to previously reported porous cyclodextrin polymers that are typically prepared as generic adsorbents for batch pollutant removal [50–52], the present sorbent was purposely engineered as an SPE phase. This was achieved by converting 2-hydroxypropyl-β-cyclodextrin into an acrylated, photopolymerizable monomer (HPCDAA) and subsequently forming a rigid, insoluble β-CD-rich network via UV-initiated radical cross-linking with ethylene glycol dimethacrylate (EGDMA). The resulting POP combines (*i*) a high density of accessible β-CD host cavities with (*ii*) a mechanically robust, regenerable porous framework compatible with cartridge-based flow-through operation, enabling high enrichment at small elution volumes and quantitative UV–Vis spectroscopic readout. Therefore, the novelty lies in the monomer-to-POP design (HPCDAA/EGDMA, UV-polymerized) yielding an SPE-tailored, β-CD-cavity-rich porous network rather than a batch-adsorbent material. This β-CD-based POP leverages the unique molecular recognition capabilities of CDs, which are known for their high affinity and selectivity towards organic pollutants. The synthesis of β-CD-derived porous polymers represents a promising approach owing to their high surface area, chemical stability, and tunable porosity, enabling superior adsorption performance compared to conventional materials. The innovative combination of β-CD functionality with porous polymer networks aims to improve enrichment efficiency and sensitivity in SPE for environmental monitoring. The morphology, surface area, and composition of the POP were characterized by scanning electron microscopy (SEM), N_2 adsorption-desorption isotherms (Brunauer-Emmett-Teller (BET) method), X-ray diffraction (XRD), thermogravimetric analysis (TGA), Fourier transform infrared (FTIR), and FT-Raman spectroscopy. The SPE process was optimized with regard to maximum enrichment of DF using DoE, i.e., a three-level-four-factor Box-Behnken design (BBD), in combination with RSM [53,54]. The maximum adsorption capacity of the developed POP was determined using the Langmuir and the Freundlich isotherms.

Furthermore, a sensitivity study for the evaluation of the method limit of detection and quantification was performed. Field emulation studies using ng/L DF concentrations in ultrapure water and seawater systems were conducted, along with analysis of the selectivity against other pharmaceutical pollutants and the regeneration capability of the material. This allows validation of the applicability of the herein proposed preconcentration method for environmental sample sensing.

2. Experimental section

2.1. Materials and methods

DF sodium (98%), ibuprofen (IBU, ≥ 98%), ethylene glycol dimethacrylate (EGDMA, 98%), 2-Hydroxypropyl)-β-cyclodextrin (HPβCD, M_w ~ 1.380), dry triethylamine (TEA, ≥ 99.5%), and acryloyl chloride (≥ 96.0%) were purchased from Sigma-Aldrich, carbamazepine (CBZ,

98%), acetylsalicylic acid (ASA, 99%,), extra dry dimethyl formamide (DMF, 99.8%, over molecular sieve, AcroSeal®), and 4-(2-Hydroxyethyl)piperazine-1-ethanesulfonic acid sodium salt (HEPES sodium salt, 99%) were purchased from Thermo Scientific. Acetonitrile (ACN, AnalR NORMAPUR Reag. Ph.Eur., ACS, ≥ 99.5%), technical grade methanol (≥ 98.5%), ethanol (EtOH, 99.5%, denaturated with 1% MEK), technical grade DMF (≥ 98%), and technical grade acetone (≥ 99%) were purchased from VWR Chemicals. (1-Hydroxycyclohexyl) phenylmethanone (HCPHM, 99.94%) was purchased from BLD Pharmatech GmbH. Analytical grade methanol (MeOH, ≥ 99.99%), analytical grade dimethyl sulfoxide (DMSO, ≥ 99.9%), glacial acetic acid (100%), 37% p.a. hydrochloric acid, and sodium hydroxide were purchased from Merck. The seawater sample (original seawater 20 L, laboratory-tested Atlantic seawater) was obtained from REBIE. The commercial SPE columns (J.T.Baker®, BAKERBOND spe™ C18 and J.T. Baker®, BAKERBOND spe™ C18 PolarPlus®) from Avantor were used for comparison with the proposed POP. According to the protocol detailed in [55], DF sodium was converted to diclofenac acid (DF) in order to obtain the neutral form of the compound. Ultrapure water (UPW) from a Sartorius system (Arium® pro, Germany) was used throughout all experiments.

2.2. Synthesis of the photopolymerizable monomer and the POP

For polymerization, the cyclodextrin derivative HPβCD was converted into a polymerizable structure. The procedure was adapted from Keutgen et al. [56] to generate an acrylated form of the polymer, which is polymerizable via radical polymerization. Briefly, dried HPβCD was reacted with acryloyl chloride via a substitution reaction to yield the acrylic structure, herein referred to as HPβCDAA (see **Fig. S1**, Supporting Information). For the synthesis of the POP, HPβCDAA (500 mg, average M_w ~ 1800.8) was dissolved in 40 mL ACN /MeOH (1/1, *v*/v). The cross-linker EGDMA (3.78 mL, 20 mmol) and the photoinitiator HCHPM (30 mg, 0.12 mmol) were added. After homogenization, radical polymerization was initiated by UV irradiation at 365 nm for 16 h. Afterwards, the final polymer was powdered, washed with MeOH/acetic acid (9/1, v/v), and dried in a vacuum oven overnight (50 °C, 600 mbar).

2.3. Physicochemical characterization methods of the synthesized monomer and the polymer

The successful functionalization of the monomer HPβCD was evaluated using ^{1}H nuclear magnetic resonance (NMR) spectroscopy (BRUKER AVANCE NEO 400 w/Bruker iProbe TBO BBFO/F/H with *Z*-Gradient Probehead). The average degree of substitution (ADS) of the acrylic monomer was calculated according to eq. (1) [57]:

$$ADS = 7\left(\frac{\int H_b}{\int H_1}\right) \quad (1)$$

$\int H_b$ represents the integral of protons introduced through successful functionalization, and $\int H_1$ represents the integral of protons originating from the initial structure prior to reaction with acryloyl chloride (**Fig. S2**, Supporting Information).

The monomer and polymer synthesized were characterized by FTIR spectroscopy in the mid-infrared region (4000–400 cm^{-1}) using a commercial FTIR spectrometer (Alpha Platinum, Bruker, Germany) equipped with a single-bounce diamond internal reflectance element. For morphological characterization, SEM micrographs (Helios Nanolab 600, Thermo Fisher Scientific, USA) were recorded at 3.0 kV and 86 pA using a through-the-lens detector. Before image acquisition, the samples were coated with platinum to form an approximately 10 nm-thick layer using a Bal-Tec SCD 005 sputter coater (Bal-Tec AG, Balzers, Liechtenstein) to reduce charging effects during SEM investigation. Powdered XRD patterns of polymer samples were recorded at room temperature on a single-crystal X-ray diffractometer (Rigaku/Oxford SuperNova) equipped with a Cu kα_1 radiation source ($\lambda = 1.540$ Å) using a generator voltage of 45 kV and a current of 40 mA. TGA was employed to analyze the degradation of the POP matrix as a function of increasing temperature (PerkinElmer TGA 8000 TM). The measurements were recorded in a dry nitrogen flow at a heating rate of 10 °C/min over a temperature range of 30–800 °C. The specific surface area and pore size distribution of the polymer were determined by BET analysis at 77.3 K using an automated N_2 gas sorption system (QuadraWin, Quantachrome, USA).

2.4. Preconcentration of DF: SPE protocol

For packing of a 3 mL empty polypropylene SPE cartridge (Bond Elut Empty SPE Cartridges, Agilent), 25 mg of the dried functional POP-based adsorbent were sandwiched between two polyethylene frits (20 μm porosity, Agilent). Any preconcentration experiment conducted herein consisted of four steps, that is conditioning, sample loading (referred to as extraction or adsorption), elution (referred to as desorption), and washing of the POP-based cartridges for adsorbent regeneration, in this order. After each step, an air purge (10 mL, 10 mL/min) was applied to prevent cross-contamination of the analyzed samples. For sample loading, standard working solutions were freshly prepared at the required concentrations prior to each experiment by diluting an initial 1000 mg/L DF stock solution in analytical-grade MeOH (stored at 4 °C) with ultrapure water (UPW) to obtain a UPW/MeOH (99/1, *v*/v) mixture. Each measurement was referenced against corresponding blank solutions, which were prepared similarly but without the addition of DF. All experiments were performed in triplicate and the results reported herein are the mean values. After completion of any SPE experiment, the liquid phases that are the applied working solution, extraction solution (effluent after adsorption), elution solution (effluent after desorption), and washing solution (effluent after washing) were analyzed with regard to their analyte concentration using UV–Vis spectroscopy. For quantification, the following calibration functions were used: in UPW/MeOH (276 nm), $y = 0.0323\times + 0.0047$, $R^2 = 0.9997$, LOD = 0.220 mg/L, LOQ = 0.666 mg/L and in MeOH (277.5 nm); $y = 0.0454\times - 0.0003$, $R^2 = 0.9996$, LOD = 0.145 mg/L, LOQ = 0.439 mg/L). The equilibrium adsorption capacity Qe (mg/g), EE (%), enrichment factor EF (a.u.), and the recovery rate R (%) were determined using the following eqs. (2)–(5):

$$Q_e\ (mg/g) = \frac{(C_i - C_e)}{m}V \quad (2)$$

$$EE\ (\%) = \frac{(C_i - C_e)}{C_i} \times 100 \quad (3)$$

$$EF = \frac{C_{elu}}{C_i} \quad (4)$$

$$R\ (\%) = \frac{m_{elu}}{m_{ext}} \times 100 \quad (5)$$

where C_i and C_e are the DF concentration (mg/L) measured in the initial working solution and after reaching adsorption equilibrium (after extraction), respectively. m is the mass of sorbent (g), V the volume of sample (L), and C_{elu} is the concentration of DF detected after elution. R is calculated by the ratio of detected mass of eluted (m_{elu}) and extracted (m_{ext}) DF from the polymer multiplied by a factor of 100. To develop a robust SPE method for preconcentration of DF prior to UV–Vis analysis, parameters that affect the performance of the set-up must be considered and optimized. Through initial literature screening, experimental variables to be considered were identified. In preliminary studies, the influence of pH on the SPE set-up was analyzed by adjusting the pH during conditioning. Furthermore, by performing OFAT experiments, the eluent type was evaluated regarding the maximum elution capability of

DF from the solid matrix. After separate assessment of these variables, the residual experimental parameters, i.e., functional POP mass, sample and elution flow rates, and elution volume were optimized utilizing a BBD approach within DoE.

2.5. Box-Behnken experimental design and procedure

To enhance the preconcentration performance of the SPE method, a systematic optimization was carried out using BBD, focusing on four critical factors (Table 1) that are the mass of the adsorbent (mg, X_1), extraction flow rate (mL/min, X_2), elution flow rate (mL/min, X_3), and elution volume (mL, X_4). Each factor was evaluated at three levels in coded form: low (−1), medium (0), and high (+1). The process response Y was defined as the EF of DF, with the main objective being the maximization of the preconcentration for subsequent quantification. The influence of the adsorbent mass, in the range of 5–25 mg, the flow rate during sample loading and elution, in the range of 1–5 mL/min, and the elution volume, in the range of 1–5 mL, were considered. For evaluation, a DF stock solution in UPW/MeOH (99/1, *v*/v) at 10 mg/L was prepared. The selection of threshold intervals for the four variables under investigation was determined through a combination of preliminary experimental results and literature data [58].

A total of 27 experimental runs with triplicates, i.e., 81 runs in total, were generated by the BBD matrix to systematically evaluate the influence of the factors and their interactions on the extraction and recovery of DF. Table 2 lists the coded and real factor values alongside the experimentally obtained EF responses. Design generation and statistical analysis were performed using STATGRAPHICS Centurion 19 (Statgraphics Technologies, Inc., Virginia, USA). In the four-factor system involving the significant independent variables X_1, X_2, X_3, and X_4, the mathematical relationship between these factors and the measured response Y was approximated using a quadratic polynomial eq. **(6)** [49].

$$Y = \beta_0 + \sum_{i=1}^{k}\beta_i X_i + \sum_{i=1}^{k}\beta_{ii} X_i^2 + \sum_{i=1}^{k-1}\sum_{j=i+1}^{k}\beta_{ij} X_i X_J \quad (6)$$

In this model, β_0 is a constant intercept term, β_i is a coefficient encountering linear effects, β_{ii} represents the quadratic effects, and β_{ij} represents the interactions between X_i and X_j [59]. Herein, positive signs indicate a positive influence on the response upon an increase in the respective parameter and vice versa. Quadratic terms, such as $\beta_{ii}X_i^2$, and factor multiplication, as in the interaction term $\beta_{ij}X_iX_j$, represent the influence of the involved factors on the response, quantifying the interdependency of the factors resulting from a simultaneous change in another factor [60].

A second-order polynomial regression in coded form was used to fit the experimental data. Solving this equation allows for estimation of the optimum values to obtain the highest EF. The importance degree of model terms was determined by the f-value and p-value. Whereby evaluation of the *p*-value allows for identification of the significance of each model. Statistical significance and correlation coefficient R^2 of the regression models for the functional POP were assessed by analysis of variance (ANOVA) with a confidence level of 95%. To gain a better understanding of the impact of the variables on the EF of DF and the interaction between them, 3D response surface graphs were prepared in Origin2019. In these graphs, two factors were kept constant while the other two factors were varied within the experimental ranges. The optimized conditions obtained from the response surface analysis were subsequently applied to the validation of the proposed SPE set-up for DF preconcentration.

Table 1
Levels of the BBD for the solid-phase extraction process.

Factor		Levels		
		-1	0	+1
X_1	Mass of adsorbent (mg)	5	15	25
X_2	Extraction flow rate (mL/min)	1	3	5
X_3	Elution flow rate (mL/min)	1	3	5
X_4	Elution volume (mL)	1	3	5

Table 2
BBD matrix in coded form and corresponding real values with the resulting EF values obtained from the respective DF SPE experiments.

Run	Factor								POP
	Coded value				Real value				Experimental value
	X_1	X_2	X_3	X_4	X_1	X_2	X_3	X_4	EF (a.u.)
1	0	0	0	0	15	3	3	3	8.49 ± 0.87
2	0	+1	0	+1	15	5	3	5	6.32 ± 0.39
3	0	-1	+1	0	15	1	5	3	10.8 ± 0.68
4	0	-1	-1	0	15	1	1	3	11.6 ± 0.08
5	+1	0	-1	0	25	3	1	3	12.5 ± 0.22
6	0	0	+1	-1	15	3	5	1	32.4 ± 2.07
7	-1	+1	0	0	5	5	3	3	3.87 ± 1.43
8	+1	0	+1	0	25	3	5	3	12.8 ± 0.20
9	+1	-1	0	0	25	1	3	3	11.9 ± 0.59
10	0	0	0	0	15	3	3	3	10.5 ± 0.46
11	0	-1	0	+1	15	1	3	5	6.28 ± 0.32
12	0	+1	-1	0	15	5	1	3	8.70 ± 0.77
13	0	0	0	0	15	3	3	3	9.44 ± 0.37
14	+1	0	0	-1	25	3	3	1	38.7 ± 1.34
15	-1	0	0	+1	5	3	3	5	3.10 ± 0.25
16	0	+1	+1	0	15	5	5	3	9.54 ± 0.71
17	0	0	+1	+1	15	3	5	5	6.08 ± 0.38
18	0	+1	0	-1	15	5	3	1	32.4 ± 2.46
19	-1	-1	0	0	5	1	3	3	6.35 ± 0.90
20	0	-1	0	-1	15	1	3	1	27.8 ± 3.09
21	+1	+1	0	0	25	5	3	3	12.1 ± 0.23
22	-1	0	+1	0	5	3	5	3	3.90 ± 1.18
23	+1	0	0	+1	25	3	3	5	7.85 ± 0.18
24	-1	0	0	-1	5	3	3	1	17.3 ± 1.38
25	0	0	-1	-1	15	3	1	1	31.2 ± 1.84
26	0	0	-1	+1	15	3	1	5	5.74 ± 0.72
27	-1	0	-1	0	5	3	1	3	5.34 ± 0.58

2.6. Comprehensive evaluation of POP-based SPE performance

To evaluate the sensitivity of the developed method, a series of DF working solutions for sample loading was prepared at concentrations of 0.1, 0.3, 1, 3, and 10 mg/L and applied in the optimized SPE set-up. In addition, a field emulation study was performed to evaluate the SPE performance at low DF concentrations. For this, a model sample solution with a DF concentration of 1500 ng/L was prepared by diluting a primary 100 mg/L methanolic solution of DF with UPW. A sample volume of 1 L was loaded onto three cartridges in consecutive triplicate measurements, with a blank as reference, using fresh cartridges for each run. The concentrations of the working solutions were confirmed by the accredited testing laboratory ZV Landeswasserversorgung (Betriebs- und Forschungslabor – organische Spurenanalytik, Zweckverband Landeswasserversorgung Langenau, Germany) in accordance with DIN EN ISO 21676:2022–01 #. Furthermore, the enrichment process was evaluated using a DF-spiked real seawater sample as the matrix. The laboratory reports on the composition of the seawater sample provided by the manufacturer are listed in **Table S1** (Supporting Information). The preparation, SPE protocol, and subsequent analysis were conducted under identical conditions to those applied in the previous model solution-based field emulation study, enabling direct comparison of the results and assessment of the applicability of the herein developed method to real-world matrices. Prior to the analysis, the methanolic eluate was filtered through a PVDF syringe filter (0.45 μm) to remove any solids originating from the seawater sample to avoid light scattering. The regeneration experiment was performed in ten adsorption-desorption cycles, with washing steps between each cycle, to analyze the material stability and method robustness. To comprehensively evaluate the performance of the as-synthesized SPE material, benchmarking against two commercial SPE cartridges, namely C18 and C18

Polar Plus, was conducted. Subsequently, the maximum adsorption capacity Q_m (mg/g) of the developed sorbent phase for DF enrichment was analyzed by applying sample solutions of DF with increasing concentrations in the range of 1–120 mg/L. Q_e for each concentration was calculated using the Langmuir model given by eq. (7):

$$Q_e = \frac{C_e K_L Q_m}{1 + C_e K_L} \quad (7)$$

and the Freundlich model given by eq. (8):

$$Q_e = K_F C_e^{1/n} \quad (8)$$

In eq. (7), K_L is the Langmuir model constant (mg/L). In eq. (8), K_F (mg/g) and *n* are the constants of the Freundlich model.

Under optimized SPE conditions, the EE of DF by the functional POP was compared to EEs of other pharmaceuticals, including IBU, CBZ, and ASA (Fig. 1), using the selectivity factor α as a descriptor (Eq. (9)):

$$\alpha = \frac{EE_{analog}}{EE_{DF}} \quad (9)$$

In Eq. (9), EE_{DF} (%) and EE_{analog} (%) are the extraction efficiencies for DF and its structural analogs, respectively. For quantification using UV–Vis spectroscopy, the other pharmaceuticals were measured at the following wavelengths: in UPW/MeOH: IBU at 221.5 nm, CBZ at 285.0 nm and ASA at 226.0 nm, and in MeOH: IBU at 220 nm, CBZ at 285.0 nm, and ASA at 226 nm. In all selectivity experiments, only one pharmaceutical was present per SPE run, and each analyte was quantified at its individual absorption maximum, thereby avoiding spectral overlap in the UV–Vis measurements. EE of the POP for each compound was calculated using Eq. (3).

2.7. Inclusion complex formation and molecular modelling of polymer-drug interaction

DF, the synthesized monomer and polymer, as well as the POP-DF composite after SPE adsorption experiments (DF concentration, 10 mg/L; sample volume, 50 mL; sorbent, 25 mg; and sample flow rate, 5 mL/min), were characterized by FTIR spectroscopy in the mid-infrared region (1800–1000 cm^{-1}), using a commercial FTIR spectrometer (Alpha Platinum, Bruker, Germany) equipped with a single-bounce diamond internal reflectance element. Raman measurements were performed on a confocal Raman microscope (WITec alpha300 R) utilizing a YAG-laser (WITec, λ = 532 nm, 1.0 mW laser power for POP and POP-DF, and 0.25 mW laser power for DF) and a VIS spectrometer (WITec UHTS 300) with a spectral resolution of ±1 rel. cm^{-1}. All measurements on the POP-DF composite were performed in triplicate. The ζ-potential of the bare POP, the POP after adsorption (DF concentration, 10 mg/L; sample volume, 50 mL; sorbent, 25 mg; and sample flow rate, 5 mL/min), and the POP in a DF spiked solution (10 mg/L) were measured using a ζ-potential analyzer (Zetasizer Nano ZS, Malvern, Germany). To ensure sufficient ionic conductivity for stable measurements, the polymer batches (5 mg each) were dispersed in a 1 mM HEPES sodium salt buffer solution (prepared in UPW; 10 mL). The suspension was sonicated for 10 min prior to each measurement.

To evaluate the intrinsic binding preferences of the amorphous polymer towards DF, molecular dynamics (MD) simulations were performed using the Schrödinger Materials Science Suite (Materials Science Suite Release 2024–4; Schrödinger, LLC: New York, NY, 2018. Schrödinger Release 2024–4 Desmond Molecular Dynamics System; Schrödinger: New York, NY, 2016). The polymer was constructed using the Polymer Builder module, generating five distinct polymer chains of acrylic HPβCD (HPβCDAA; **Fig. S1**, Supporting Information), each consisting of five monomeric units and then cross-linked with EGDMA. This configuration was chosen to consider balance between computational feasibility and structural complexity in molecular simulation studies of cross-linked or amorphous polymer systems. To mimic the experimental solubilization environment, the Disordered System Builder was employed to randomly distribute 200 drug molecules, 5000 water molecules, and 50 MeOH molecules around the polymeric network. This solvent composition was chosen based on the experimental condition in which the drug was solubilized in a 99/1 (*v*/v) UPW/MeOH system, thereby providing a closer approximation of the solution-phase behavior observed during loading and interaction studies. Following system preparation and minimization, 100 ns of all-atom MD simulations were carried out under isothermal-isobaric conditions using the OPLS4 force field. Periodic boundary conditions were applied for long-range electrostatics. Only non-covalent interactions between the polymer and the drug molecules were retained for post-simulation analysis. Solvent molecules and intramolecular drug interactions were excluded to focus on the specific types and number of interactions, primarily hydrogen bonds, halogen bonds, and hydrophobic contacts, governing the polymer-drug recognition.

3. Results and discussion

3.1. Physicochemical characterization results of the synthesized monomer and polymer

Successful formation of HPβCDAA was validated by relevant peak assignment, which are the anomeric H^1 proton originating from the unchanged α-D-glycopyrolose backbone and the incorporated vinyl protons in the acrylic moiety, in a ^{1}H NMR spectrum in comparison to unreacted HPβCD (**Fig. S2**, Supporting Information) [61].

The broad multiplets appearing between 6.1 and 5.1 ppm are caused by the protons H^b and H^1, respectively [61] (**Fig. S2**, Supporting Information). The corresponding integrals are set in relation according to **Eq. (1),** yielding an ADS of 1.84. The structural characteristics of the synthesized functional POP were evaluated using FTIR spectroscopy (Fig. 2a). The band at 3745 cm^{-1} corresponds to the stretching vibrations of O—H from the hydroxyl groups present in the β-CD moiety [62]. The absorption band at 2974 cm^{-1} corresponds to C—H stretching in aliphatic chains [62]. A weak band near 2370 cm^{-1} may relate to atmospheric CO_2 or residual monomeric species [63]. A pronounced band at approximately 1723 cm^{-1} is linked to the C═O stretching vibration of ester groups, resulting from the cross-linking agent EGDMA. Additionally, the band observed at 1159 cm^{-1} is attributed to C—O stretching vibrations from the CD backbone. These findings align with the anticipated polymer structure. The XRD data presented in Fig. 2b indicate an amorphous character of the analyzed polymer, as no distinct diffraction patterns were observed. During TGA of the POP material, an initial weight loss observed around 46 °C (Fig. 2c) was attributed to the evaporation of residual solvent molecules (mainly ethanol) weakly

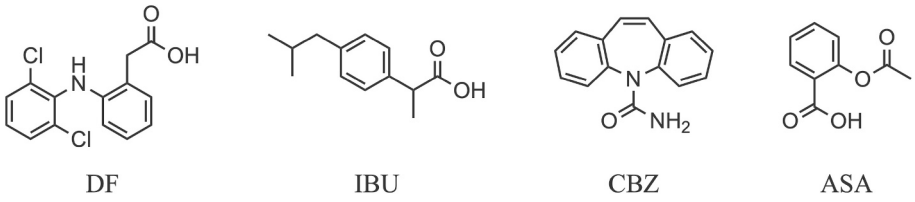

Fig. 1. Structure of DF and the other analyzed pharmaceuticals IBU, CBZ, and ASA.

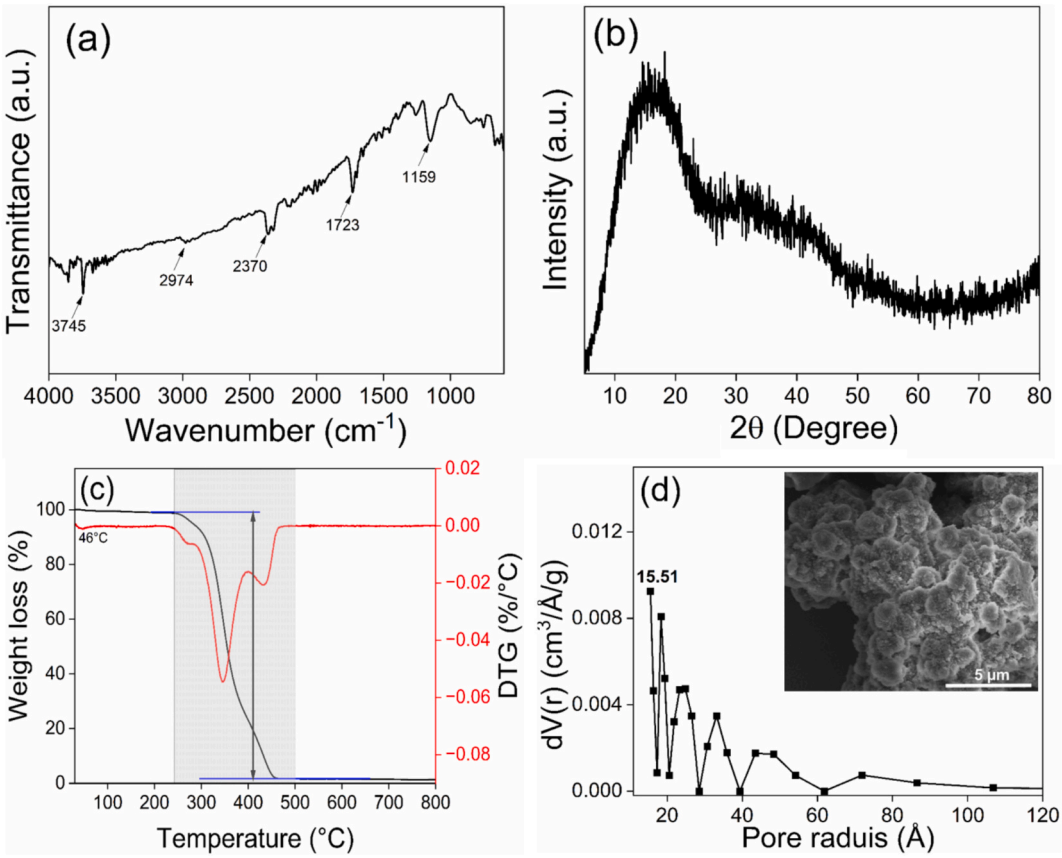

Fig. 2. (a) FTIR spectra of the POP recorded in ATR mode with a single-bounce diamond crystal over 400–4000 cm^{-1}. (b) Powder-XRD patterns collected on a single-crystal X-ray diffractometer using a Cu Kα₁ radiation (λ = 1.540 Å, 45 kV and 40 mA). (c) TGA and DTG curves measured under N_2 at a heating rate of 10 °C/min from 30 to 800 °C, and (d) pore size distribution derived from N_2 sorption isotherms recorded at 77 K for the POP: The inset: SEM image of the Pt-coated POP, acquired at 10000-fold magnification (3.0 kV accelerating voltage, 86 pA beam current, through-the-lens detector).

retained in the polymer network or trapped within the β-CD cavities (1.45 wt%), which was used during synthesis and washing. Between 250 and 500 °C, the most pronounced mass loss was observed. This mass loss occurred in three phases, with the inflection points being at 270 °C, 340 °C, and 426 °C. The losses, between approximately 250 °C and 500 °C are associated with the degradation of the hydroxypropyl groups and the cyclodextrin backbone, respectively.

The overall mass loss of the polymer in this temperature range was 98.45 wt%. The morphological characteristics of the synthesized polymer were analyzed using SEM, as depicted in the inset of Fig. 2d. The micrograph shows tightly packed, aggregated, round particles with a relatively dense structure and minimal visible porosity. The porosity and specific surface area of the adsorbent were assessed via BET analysis. The adsorbent possesses a specific surface area of 46.80 m^2/g, a total pore volume of 0.137 cm^3/g, and a pore radius of 15.51 Å, indicating that a pore possesses at least one β-CD moiety, as the outer rim of one molecule is 15.4 Å [33]. Furthermore, the pore size distribution was analyzed. The prepared polymer displays several pore diameter peaks at 15.51, 18.32, 24.84, 33.13, 43.45, and 71.9 Å, typical for cross-linked polymers generated using radical polymerization [64].

3.2. SPE process

3.2.1. Preliminary studies

The binding of DF acid to the hydrophobic cavity of a CD moiety is preferred over the binding of its salt conformation due to the increased hydrophobicity of the acidic species. Therefore, DF sodium was converted to DF acid for use in this study [65]. For desorption of DF from the functional POP, various eluents were investigated, including ACN, MeOH, EtOH, DMSO, and DMF (see **Fig. S3,** Supporting Information). Among them, MeOH showed the best desorption behavior of DF from the synthesized material, thus it was selected for elution of the analyte. This is in accordance with the high solubility of DF in MeOH [65]. Furthermore, MeOH is considered a less hazardous solvent compared to DMSO and DMF, making it preferable as an eluent [66]. To assess the impact of pH changes on the enrichment process of DF, experiments under acidic conditions at pH = 2, in contrast to neutral pH, during conditioning were conducted. Since β-CD is a neutral host molecule (pK_a(β-CD) = 12.2), the pH responsiveness of the material is negligible [33]. On the contrary, protonation of DF at pH values below its pK_a value of approximately 4.0–4.5 leads to a higher non-polar character than in the deprotonated form, thus increasing the complex stability [65,67]. Additionally, according to A. A. Abdoh et al., the interaction between neutral DF is highest with HPβCD, as the peripheral hydroxypropyl groups allow for flexible interaction with both the phenylacetic acid, as well as the stereochemically more demanding dichlorophenyl moiety, which are not provided by the more rigid 1:1 complexation by β-CD (only interaction with the phenylacetic acid group). The strongest host-guest binding occurs between HPβCD and DF acid in acidic conditions. The $K_{1:1}$ in acidic media is 2.61 times higher compared to at pH 6.5 [65]. The results summarized in **Table S2** (Supporting Information) indicate that, under the chosen conditions, the elution process of DF after acidic pretreatment of the cartridge was hindered due to enhanced interaction between the analyte and the solid-phase, hence leading to decreased EF and R values, which is even halved. Consequently, pH adjustments were no longer considered in the DoE and all subsequent experiments were performed at neutral pH.

3.2.2. Optimization of SPE parameters using DoE

To improve DF enrichment, the SPE method was optimized using a systematic DoE strategy. All experimentally obtained EF values during BBD are listed in Table 2. Corresponding EE, Qe, and R values are presented in **Table S3** (Supporting Information). The empirical relationship between the EF of DF and the four variables, as well as their interactions, is given by eq. (10).

$$Y_{EF-POP} = 29.84 + 1.32X_1 - 0.32X_2 - 1.28X_3 - 14.83X_4 - 0.013X_1^2 + 0.033X_1X_2 + 0.022X_1X_3 - 0.209X_1X_4 + 0.051X_2^2 + 0.096X_2X_3 - 0.283X_2X_4 + 0.142X_3^2 - 0.058X_3X_4 + 2.16X_4^2 \quad (10)$$

The ANOVA results (Table 3) show that the statistical model performs very well in describing EF as a function of the experimental parameters studied. The coefficient of determination, R^2 = 97.3%, indicates that the model explains almost all the variability in response. This result is corroborated by an adjusted R^2 value of 96.56%, which accounts for the number of variables included in the model, as well as by a predicted R^2 value of 95.53%, indicating strong predictive performance for untested data points. These high values underline the robustness and reliability of the model. The ANOVA results demonstrate that adsorbent mass (X_1) and elution volume (X_4) are the two most influential variables for optimizing EF, with the highest f-values of 226.06 and 1508.41, respectively, with *p*-values <0.0001. Elution volume also showed a significant non-linear effect (X_4^2, f-value = 345.95, p-value <0.0001, probably due to a trade-off between maximum recovery and dilution. Similarly, adsorbent mass has a significant quadratic effect (X_1^2, p-value = 0.0067), indicating an optimal point, beyond which EF decreases or reaches a plateau. The interaction between mass and elution volume (X_1X_4, f-value = 60.46, p-value <0.0001) is also highly significant, suggesting that their effects are interdependent. In contrast, the other main effects and interactions tested are negligible (*p*-value >0.05), allowing simplification of the model. In terms of statistical performance, the standard error of the estimate of 1.86 and the mean absolute error of 1.30 show that the differences between experimentally observed values and those predicted by the model are small, confirming good accuracy. In addition, the Durbin-Watson test (2.39; p-value = 0.93) indicates the absence of significant autocorrelation in the residuals, reinforcing the validity of the model for the analysis of this type of experimental data. The correlation plots of model predictions against experimental results for the response Y_{EF-POP} are shown in Fig. 3. The high R^2 value of 0.972 indicates a robust fit between predicted and experimental data and proves that the EF, as well as the main contributing variables, can be predicted effectively by the model equations based on the chosen independent variables.

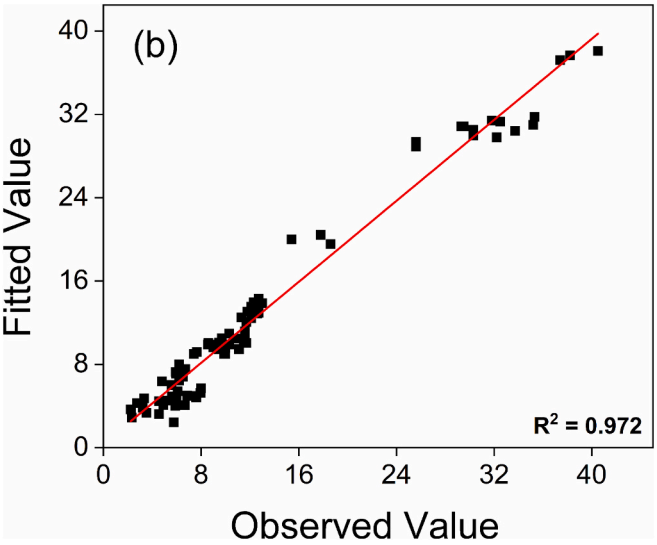

Fig. 3. Correlation plot of the model-predicted versus experimentally observed EF values, showing the statistical significance and quality of fit of the quadratic response surface model, as confirmed by ANOVA.

The 3D plots (Fig. 4) show the dependency of EF on the adsorbent mass and the sample flow rate, on the adsorbent mass and the elution volume, and on the sample and elution flow rates. The 3D response surface plots facilitate a straightforward visualization and examination of the effects of the experimental factors on the responses [68]. Fig. 4a shows that increasing sorbent mass and sample flow rate lead to an overall increase in EF, also seen in the RSM graph Fig. 4b. This suggests a larger amount of sorbent enhances DF retention due to an increasing amount of available binding sites, while a higher sample flow rate improves mass transfer up to a certain threshold. In Fig. 4b, a stark interaction between POP mass and elution volume is observed. The EF reaches its maximum at the lowest elution volume (1 mL), indicating that excessive eluent volumes dilute DF and consequently reduce the EF. The EF remains relatively stable across most flow rate combinations, whereas increasingly high elution flow rates reduce the efficiency, probably due to insufficient contact time with the solid-phase (Fig. 4c). The Pareto diagram (see Fig. 4d) highlights the relative importance of each factor and their interactions on the EF. The factor X_4 (elution volume) is by far the most influential, followed by sorbent mass (X_1) (results confirmed by ANOVA). Cross-interactions, although less pronounced, are not negligible and must be taken into account during optimization. These results highlight the robustness and reliability of the regression model used to optimize the conditions for preconcentrating DF, confirming that the experimental data closely match the developed model. After feeding the output data into the DoE software, the optimum conditions predicted by employing eq. (10) for maximizing the EF (EF = 38.30) were determined to be sorbent mass of 25 mg, a sample flow rate of 5 mL/min, an elution flow rate of 1 mL/min, and an elution volume of 1 mL. The predicted EF was associated with lower and upper 95% confidence limits of 37.39 and 43.46, respectively.

For the validation of the DoE results, the optimized conditions were applied to three consecutive SPE cycles. Based on the results presented in Table 4, DF was nearly completely adsorbed by the POP (98.50 ± 0.35%), indicating suitable affinity of the prepared polymer towards DF. After elution with 1 mL of MeOH, 78.70 ± 0.35% of DF was recovered. The DF amount in the sample was thereby enriched by a factor of 38.8 ± 1.58, yielding a final concentration of 373.5 ± 14.7 mg/L. For three

Table 3
ANOVA results for the quadratic response surface model of DF preconcentration using POP.

Source	Sum of square	Degree of freedom	Mean square	f-value	p-value
X_1	780.83	1	780.83	226.06	0
X_2	0.877344	1	0.877344	0.25	0.616
X_3	0.087025	1	0.087025	0.03	0.8744
X_4	5210.19	1	5210.19	1508.41	0
X_1^2	27.1499	1	27.1499	7.86	0.0067
X_1X_2	5.26687	1	5.26687	1.52	0.2214
X_1X_3	2.36741	1	2.36741	0.69	0.4108
X_1X_4	208.834	1	208.834	60.46	0
X_2^2	0.6552	1	0.6552	0.19	0.6646
X_2X_3	1.8252	1	1.8252	0.53	0.4699
X_2X_4	15.3907	1	15.3907	4.46	0.0387
X_3^2	5.14282	1	5.14282	1.49	0.2269
X_3X_4	0.644033	1	0.644033	0.19	0.6673
X_4^2	1194.93	1	1194.93	345.95	0
blocks	10.6947	2	5.34736	1.55	0.2205
Total error	221.062	64	3.45409		
Total (corr.)	8036.89	80			

R^2 = 0.973, adjusted R^2 = 0.966, predicted R^2 = 0.955.

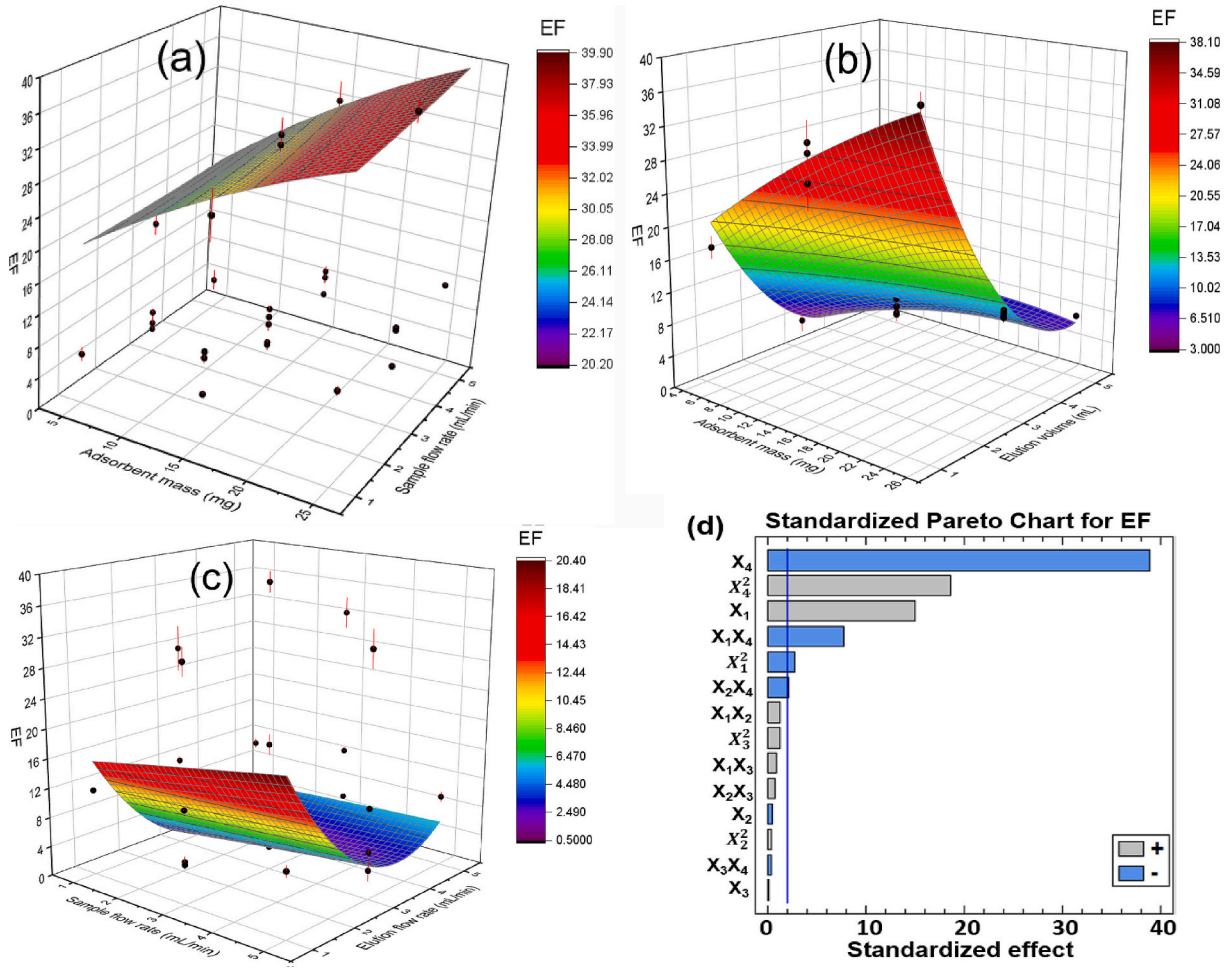

Fig. 4. 3D response surface plots of the effects of: (a) POP mass and sample flow rate with $X_3 = 3$ mL/min and $X_4 = 1$ mL, (b) POP mass and elution volume with $X_2 = 3$ mL/min and $X_3 = 3$ mL/min, and (c) sample and elution flow rates with $X_1 = 25$ mg and $X_4 = 1$ mL on EF. (d) Pareto Chart of factor effects. All experiments used 50 mL of a 10 mg/L DF solution in UPW/MeOH (99/1, *v*/v), with MeOH elution (1 mL); data points are mean values ± SD ($n = 3$), quantified by UV–Vis spectroscopy.

Table 4
Validation of the BBD-predicted optimal SPE conditions and statistical evaluation of POP performance for DF binding.

	EE (%)	Qe (mg/g)	EF	R (%)
POP	98.5 ± 0.350	19.0 ± 0.10	**38.80 ± 1.58**	78.70 ± 3.44
RSD	0.355	0.499	**4.08**	4.37

consecutive measurements, EE, Qe, EF, and R values remained within the 95% confidence range. These results confirm the reliability and predictive accuracy of the DoE model, demonstrating the effectiveness and robustness of the SPE process optimized for DF enrichment under the conditions tested.

3.2.3. *Comprehensive evaluation of POP-based SPE performance*

To evaluate the sensitivity of the optimized method, the preconcentration behavior was analyzed over a concentration range of 0.1–10 mg/L. A linear relationship between the applied initial concentration and the measured eluted concentration was observed (see **Fig. S4**, Supporting Information), which is expressed by the following equation: $y = (41.74 \pm 0.86)x + (0.32 \pm 0.25)$ with $R^2 = 0.998$, where x and y are the initial and eluted concentration of DF, respectively. The method limit of detection (MLD), as well as the method limit of quantification (MLQ), were determined according to IUPAC guidelines, using the 3σ/slope and 10σ/slope approaches, where σ represents the standard deviation of the blank [66]. The calculated MLD and MLQ values were 18.0 ± 0.4 μg/L and 59.9 ± 1.2 μg/L, respectively. For each concentration tested, the EE, Qe, EF, and R were assessed (**Table S4**, Supporting Information). Both adsorption and desorption processes occurred with near-complete efficiency, confirming the effectiveness of the conditions and supporting the reliability of the analytical method. These sensitivity values reflect the performance of the SPE-UV–Vis method for the enrichment of DF from 50 mL aqueous samples under controlled conditions.

For environmentally relevant concentrations in the ng/L to μg/L range, the analyte can be transferred into the UV–Vis working range by increasing the sample volume while maintaining a low elution volume, as demonstrated by the performed field emulation experiments. Within these studies aqueous DF samples, with a sample volume of 1 L at initial sample concentrations of 1500 ng/L, were used to evaluate the effectiveness of the developed porous polymer within the optimized SPE setup (Fig. 5) (sorbent mass, 25 mg; sample flow rate, 5 mL/min; elution flow rate, 1 mL/min; elution volume, 1 mL). The preconcentration behavior was tested using DF-spiked UPW-based model solutions in contrast to complex real seawater samples. The analysis of the model system revealed average DF concentrations within the eluate (MeOH) of 0.971 ± 0.239 mg/L, corresponding to a recovered mass of 971 ± 239 ng, EF of 647 ± 159, and R of 64.7 ± 15.9%. In comparison, a DF concentration of 0.824 ± 0.0396 mg/L was detected within the desorption solution of the seawater sample, yielding an EF of 549 ±

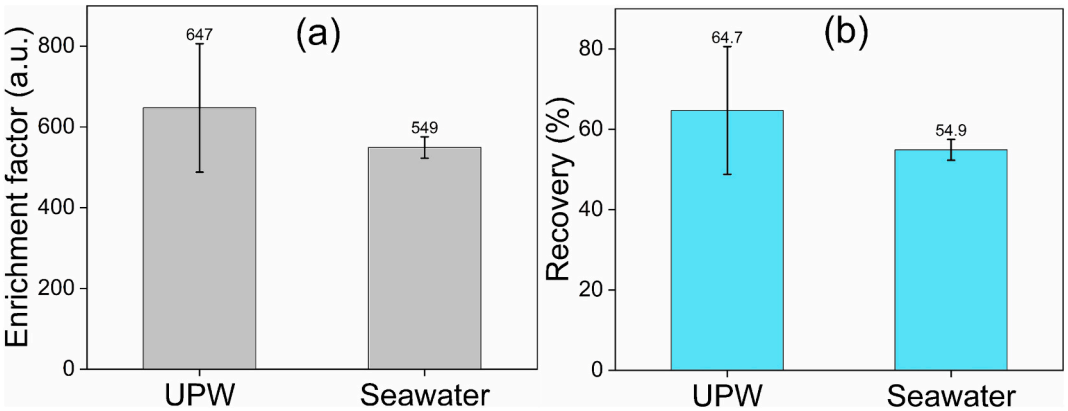

Fig. 5. Field-emulated preconcentration of DF (1500 ng/L, 1 L) by the POP in different aqueous matrices (ultrapure water (UPW) and seawater) under optimized SPE conditions (sorbent, 25 mg; sample flow rate, 5 mL/min; elution flow rate, 1 mL/min; and elution volume, 1 mL). (a) Enrichment factors. (b) Recoveries. Data represent mean ± SD (n = 3), eluates were quantified by UV–Vis spectroscopy.

26.43. With the similar assumption that all of the DF was adsorbed during sample loading, a recovery of 54.9 ± 2.64% was achieved (Fig. 5).

These findings indicate that the proposed enrichment method yields comparable EF and R values for the DF-spiked UPW-based model solution relative to the real seawater sample (ΔEF = 98; ΔR = 9.8%). Despite R of less than 80%, these results demonstrate a strong preconcentration capability at environmentally relevant trace levels, highlighting the suitability of the POP for monitoring pharmaceutical contaminants in real-world and complex matrix applications.

During evaluation of the regeneration capability of the solid matrix, only a slight reduction in adsorption capability, i.e., EE and Qe, was observed (**Fig. S5**, Supporting Information). Qe decreased by 0.292 mg/g and the EE decreased from 99.65% to 98.30% (ΔEE = 1.35%). Overall, the POP maintained a high absolute adsorption performance after ten consecutive cycles (21.53 mg/g), thus demonstrating good structural stability and further confirming its suitability as an adsorbent for water treatment. These results highlight the suitable adsorption characteristics of the synthesized material even after repeated use.

As shown in **Fig. S6** (Supporting Information), the C18 materials adsorbed significantly less DF (76.35 ± 1.98–88.1 ± 2.89%) compared to the prepared POP (98.75 ± 1.75%). Consequently, the desorbed DF concentrations and, thus, the EFs were also lower (277 ± 9–313 ± 9 mg/L for C18/C18 PolarPlus vs. 373 ± 15 mg/L for POP). The weaker retention observed for C18 phases may result from their reliance on only non-polar C—H functionalities to form Van der Waals type interactions, as previously reported [69]. This experiment revealed better binding behavior of DF towards the prepared adsorbent material when benchmarked against conventional C18 materials.

To evaluate the maximum Qe of 25 mg of the sorbent, SPE experiments with concentrations ranging from 1 to 120 mg/L were carried out (Fig. 6a and Table 5), yielding a maximum adsorption capacity of Qm = 143.49 ± 8.64 mg/g according to the Langmuir model. With a high coefficient of determination of (R^2 = 0.97), the Langmuir model provides an excellent fit to the experimental data, indicating that adsorption likely occurs predominantly as a monolayer on homogenous sites [70]. In contrast, the Freundlich constants (n > 1) indicate favorable adsorption.

To further validate the relevance of the herein proposed method for preconcentration of other drug pollutants from aqueous matrices, the material was also tested for the removal of IBU, CBZ, and ASA (see Fig. 6b). Stock solutions of each pharmaceutical (10 mg/L) were prepared and used for sample loading within the optimized SPE set-up. Compared to the nearly complete adsorption of DF (EE = 97.60 ± 0.18%, RSD = 0.182%), IBU was also adsorbed efficiently (EE = 95.50

Table 5
Adsorption isotherm model parameters for DF adsorption of POP.

Sorbents	Langmuir isotherm model			Freundlich isotherm model		
Parameter	Q_m (mg/g)	K_L (mg/L)	R^2	n	K_F (mg/g)	R^2
POP	143.49 ± 8.64	1.27 ± 0.30	0.97	6.03	73.10 ± 12.83	0.74

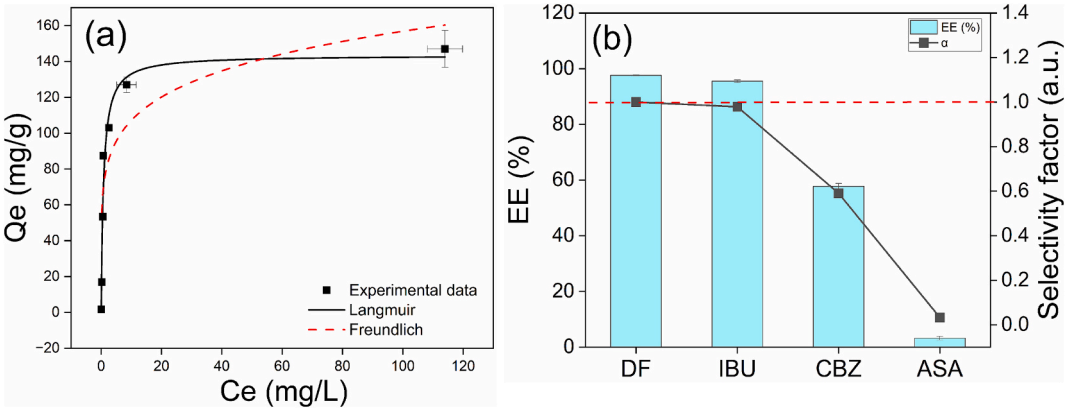

Fig. 6. (a) DF adsorption isotherm on the POP under optimized SPE conditions (sorbent, 25 mg; sample flow rate, 5 mL/min; elution flow rate, 1 mL/min; and elution volume, 1 mL), with non-linear Langmuir and Freundlich fits. (b) Extraction efficiencies and selectivity factors for DF, IBU, CBZ, and ASA. All experiments used 50 mL of a 10 mg/L analyte solution in UPW/MeOH (99/1, v/v), with MeOH elution (1 mL); data are mean ± SD (n = 3), quantified by UV–Vis spectroscopy.

± 0.44%, RSD = 0.464%), yielding a selectivity factor of α = 0.979. This high EE is likely due to structural similarity, comparable lipophilicity, and comparable physicochemical properties as these NSAIDs share a carboxylic acid functional group and similar hydrophobic aromatic ring [71]. Both DF (log P = 4.51) and IBU (log P = 3.97) display high lipophilicity, enabling favorable interactions with the hydrophobic β-CD cavity. In contrast, CBZ and ASA demonstrated much lower EEs of 57.7 ± 1.05% (RSD = 1.81%, α = 0.591) and 3.23 ± 0.68% (RSD = 21.0%, α = 0.0331), respectively. The more than 30-fold difference between EE of DF and that of ASA clearly demonstrates the polymer selectively forms inclusion complexes with chemicals similar to DF. This selectivity is rationalized not only by structural differences but also by marked disparities in lipophilicity: CBZ (log P = 2.77) and particularly ASA (log P = 1.18) do possess considerably lower lipophilicity compared to DF. The lower lipophilicity of these compounds reduces their hydrophobic interactions with the β-CD cavity, diminishing binding affinity and adsorption efficiency. Another factor contributing to the observed selectivity trend is the differential water solubility of the analytes. The decrease in extraction efficiency of the β-CD-based POP towards DF, IBU, CBZ, and ASA correlates inversely with their aqueous solubility. With increasing water solubility, enhanced solvation of the analytes by water molecules preferentially stabilizes them in the aqueous phase, decreasing their affinity for the adsorbent material and thus reducing Qe. DF and IBU, as relatively hydrophobic NSAIDs with limited aqueous solubility, readily partition from the aqueous solution onto the hydrophobic binding sites of the POP. Conversely, the higher water solubility of CBZ and especially ASA, which exhibits the highest aqueous solubility among the four compounds, implies that these molecules are preferentially solvated by water, creating an energetic barrier to their adsorption onto the hydrophobic POP surface. This solvation effect, combined with the lower lipophilicity of these compounds, synergistically reduces their affinity towards the polymer material. According to literature, all pharmaceuticals used herein form inclusion complexes with β-CD or its derivatives [43–45,65,72–77]. The reported K_A values described in previous studies for host-guest complexes with DF, IBU, CBZ, and ASA vary considerably, reflecting differences in molecular structure and steric compatibility with the host cavity. The more hydrophobic compounds DF and IBU tend to show stronger interaction towards the host, typically ranging from 10^3 to 10^4 M^{-1}, due to their favorable fit within the β-CD cavity [43–45,65,72–74,77], whereas the comparatively more hydrophilic CBZ and ASA show weaker inclusion (10^2–10^3 M^{-1}) [45,72,75,76]. Moreover, the ionization state of the analytes, determined by the pH of the aqueous matrix, further influences interaction strength. Accordingly, the selectivity observed for the present HPβCD-based host is consistent with the reported K_A and log P values of the compounds [43,65,72,73,76]. These findings are reflected by a drop in the selectivity factor from α = 0.979 for the similarly lipophilic IBU to α = 0.591 for CBZ and α = 0.0331 for ASA. This behavior quantifies progressively stronger discrimination as both molecular structure and lipophilicity diverge from those of DF. Collectively, these results validate the applicability of the HPβCD-based POP for selective pharmaceutical monitoring in environmental waters. In the present selectivity experiments, potential UV–Vis interference is intrinsically minimized, since each SPE run contains an individual analyte, which is quantified at its own absorption maximum, thereby preventing spectral overlap. For complex multi-analyte samples in which co-eluted UV-absorbing species at 276–277.5 nm may be present, the POP is best used as a preconcentration and clean-up step prior to chromatographic separation (e.g., HPLC-UV or LC-MS/MS) to ensure unequivocal DF quantification. The comprehensive selectivity study indicates preferential binding of the β-CD-functionalized POP towards DF and structurally related compounds such as IBU, driven by complementary molecular fit, high K_A values for host-guest complex formation, and lipophilic matching, thereby highlighting its potential as a selective and robust adsorbent for monitoring pharmaceutical pollutants in environmental samples.

3.3. Inclusion complex formation and molecular modelling of polymer-drug interaction

To provide experimental evidence of the inclusion of DF within the POP and to rationalize the adsorption mechanism, the materials were analyzed by ATR-FTIR and Raman before and after the SPE process under optimized conditions (DF concentration: 10 mg/L; sample volume: 50 mL; sorbent: 25 mg; flow rate: 5 mL/min). **Fig. S7** (Supporting Information) presents the ATR-FTIR spectra of the POP, DF, and POP-DF in the spectral range 1800–1000 cm^{-1}. DF shows characteristic absorption bands at 1578 and 1505 cm^{-1} assigned to the asymmetric and symmetric stretching vibrations of the carboxylate group (COO^-), together with aromatic C═C modes in the 1600–1400 cm^{-1} region and C–N/C–O vibrations between 1200 and 1000 cm^{-1} [78,79]. After adsorption, the POP-DF spectrum exhibits new and intensified bands in the 1600–1400 cm^{-1} region that match the DF fingerprint, while the ester C═O band of the polymer slightly decreases in intensity and shifts. These changes indicate intermolecular interactions, such as hydrogen bonding or ionic interactions, between the DF carboxylate and functional groups of the polymer, confirming successful incorporation of DF without alteration of the polymer backbone. Complementary results were obtained via Raman spectroscopy (Fig. 7a). In the region of interest (1550–1630 cm^{-1}), two DF-specific bands at 1593 and 1615 cm^{-1}, attributed to the stretching vibrations of the dichlorophenyl and phenylacetate rings, are clearly observed in the POP-DF spectrum (Fig. 7b) [80]. The slight shifts in these peak positions compared to pure DF further support the presence of specific host-guest interactions within the.

HPβCD cavities. These spectroscopic findings verify that the moieties act as the functional binding sites for DF inclusion. The presence of HPβCD within the POP as a functional binding moiety for DF inclusion was verified by ATR-FTIR and FT-Raman analyses of the sorbent (**Fig. S7**, and Fig. 7), indicating successful incorporation of the functional monomer HPβCDAA into the polymer matrix during free-radical polymerization.

The measured weakly negative ζ-potential of −16.6 ± 6.27 mV for the POP is consistent with values reported in the literature for CD-based polyacrylate matrices [81–84]. The recorded negative ζ-potential is attributed to the preferential adsorption of hydroxide ions from the aqueous medium onto the hydrophobic interface [84,85]. After interaction with DF, a shift towards more negative ζ-potential values was observed. The POP analyzed after DF adsorption exhibited a value of −17.9 ± 4.46 mV, whereas pure POP dispersed in a DF solution showed −22.8 ± 5.21 mV. The presence of anionic or partially negatively charged molecules can therefore increase the magnitude of the negative surface potential through adsorption at the particle interface [81,82,84]. Due to host-guest interactions between the hydrophobic aromatic moiety of DF and the hydrophobic cavity of the CD-derivative, the carboxylate group of the guest is oriented towards the bulk solution, thereby increasing the negative charge density at the shear plane [81,82,84].

To rationalize the experimental selectivity patterns at the molecular level, all-atom MD simulations were carried out for the disordered HPβCD polymer in mixed solvent environments. Each simulated system included explicit solvent molecules (water and MeOH) to mimic realistic experimental conditions. During post-processing, only the drug-polymer complex was analyzed to elucidate how polymer conformational flexibility, functional group orientation, and local microenvironment collectively influence selective binding. DF exhibited the most diverse interaction profile with the polymer matrix (**Fig. S8**, Supporting Information). Structurally, DF consists of a dichlorophenyl ring linked via an amine functionality to a phenylacetic acid moiety, providing multiple functional groups capable of forming preferential interactions. The MD trajectory (Fig. 8) revealed that the carboxylate group of DF frequently forms strong hydrogen bonds (shown in yellow) with hydroxyl groups of the β-CD units, anchoring the molecule at the polymer interface.

Notably, the chlorine atoms on the dichlorophenyl ring participate in

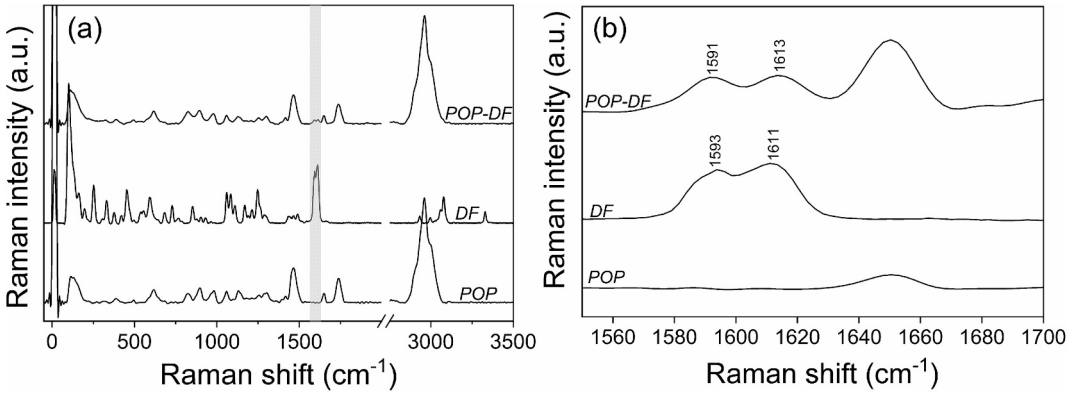

Fig. 7. FT-Raman spectra of the POP, DF, and POP-DF in the (a) 0–3500 cm^{-1} and 1550–1700 cm^{-1} spectral range.

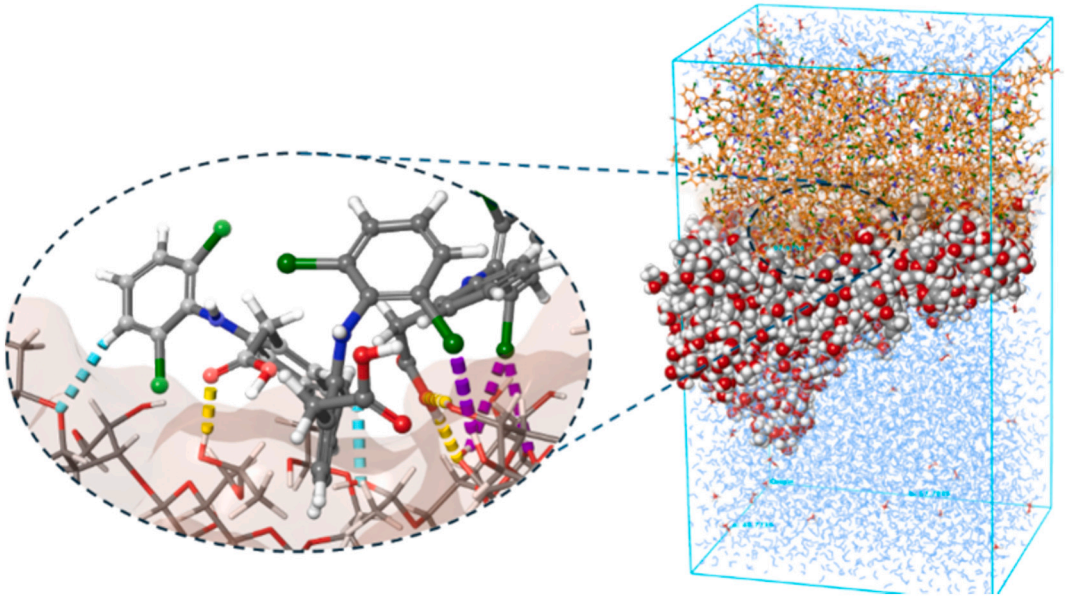

Fig. 8. Molecular dynamics snapshot of DF adsorption on the polymer network in a water-MeOH mixture. The polymer is shown in space-filling mode (O: red, C: white), DF in yellow sticks, and solvent as blue lines. Inset: interfacial binding highlights key non-covalent interactions, hydrogen (yellow), halogen (purple), and aromatic bonds (light blue) that stabilize drug adsorption. (For interpretation of the references to colour in this figure legend, the reader is referred to the web version of this article.)

halogen bonding (highlighted in purple) with electron-rich sites, such as carbonyl or ether oxygen atoms within the polymer network. These halogen bonds, with interaction strengths comparable to those of hydrogen bonds, provide directionality and enhance the overall affinity of DF for the binding cavity. Hydrophobic contacts also contribute to the stabilization of the drug within the non-polar regions of the β-CD-EGDMA polymer. Overall, the combination of multiple hydrogen bonds, directional halogen bonding, and hydrophobic interactions establishes a robust and complementary interaction pattern between DF and the polymer matrix. This cooperative interplay explains the experimentally observed preferential and strong binding affinity of DF compared to other drugs.

4. Conclusion

In this study, we successfully developed a simple, selective, and environmentally friendly analytical strategy for the detection of DF in aqueous samples, based on a functional POP bearing host-guest binding sites, which are provided by a β-cyclodextrin derivative. The combination of supramolecular binding, SPE, and UV–Vis spectroscopy, with a strategic DoE-based optimization protocol, resulted in a robust, reproducible, and selective method. The POP exhibited excellent binding performance, confirmed by both experimental characterization and computational studies. MD simulations further revealed that the enhanced affinity of DF arises from the cooperative interplay of hydrogen and halogen bonding interactions within the β-CD-EGDMA polymer matrix, providing molecular-level validation of the observed selectivity. The promising performance of this HPβCD-containing POP suggests wider applications in environmental and pharmaceutical analysis. Future work will focus on miniaturizing the system for on-site analysis, integrating it into a portable detection platform and thus enabling straightforward in-line detection and quantification of DF or other contaminants in continuous water quality monitoring systems.

CRediT authorship contribution statement

Amelie Huber: Writing – review & editing, Writing – original draft, Investigation, Data curation. **Soumya Rajpal:** Writing – review & editing, Writing – original draft, Investigation. **Dionysis Adamou:** Writing – review & editing, Validation, Investigation. **Panayiota Demosthenous:** Writing – review & editing, Validation. **Buse Parlak:** Investigation, Data curation. **Selis Onel:** Writing – review & editing,

Validation. **Boris Mizaikoff:** Writing – review & editing, Project administration, Funding acquisition, Conceptualization. **Sherman Lesly Zambou Jiokeng:** Writing – review & editing, Writing – original draft, Validation, Methodology, Conceptualization.

Declaration of competing interest

The authors declare that they have no known competing financial interests or personal relationships that could have appeared to influence the work reported in this paper.

Acknowledgments

This work was funded by the EU Horizon 2020 project ENVIROMED (Grant No. 101057844), which focuses on developing a next-generation toolbox for greener pharmaceutical design and manufacturing to reduce environmental impact. We thank the Open Access Publishing Fund of the University of Ulm for funding. Special thanks are extended to Dr. Gregor Neusser at the Focused Ion Beam Center UUlm (Institute of Analytical and Bioanalytical Chemistry, Ulm University, Germany) for assistance with the SEM studies and to Dipl.-Ing. (FH) Sabine Junginger at ZV Landeswasserversorgung (Betriebs- und Forschungslabor – organische Spurenanalytik, Zweckverband Landeswasserversorgung Langenau, Germany). The authors acknowledge Simon Schauer for enabling Raman spectroscopy analysis at the Institute for Inorganic Chemistry II at Ulm University. The authors also acknowledge support by the state of Baden-Württemberg through bwHPC and the German Research Foundation (DFG) through Grant no INST 40/575-1 FUGG (JUSTUS 2 cluster).

Appendix A. Supplementary data

Supplementary data to this article can be found online at https://doi.org/10.1016/j.microc.2026.117712.

Data availability

Data will be made available on request.

References

[1] J. Rivera-Utrilla, M. Sánchez-Polo, M.Á. Ferro-García, G. Prados-Joya, R. Ocampo-Pérez, Pharmaceuticals as emerging contaminants and their removal from water. A review, Chemosphere 93 (2013) 1268–1287, https://doi.org/10.1016/j.chemosphere.2013.07.059.

[2] B. Petrie, R. Barden, B. Kasprzyk-Hordern, A review on emerging contaminants in wastewaters and the environment: current knowledge, understudied areas and recommendations for future monitoring, Water Res. 72 (2015) 3–27, https://doi.org/10.1016/j.watres.2014.08.053.

[3] A.C. Collier, Pharmaceutical contaminants in potable water: potential concerns for pregnant women and children, EcoHealth 4 (2007) 164–171, https://doi.org/10.1007/s10393-007-0105-5.

[4] L.H.M.L.M. Santos, A.N. Araújo, A. Fachini, A. Pena, C. Delerue-Matos, M.C.B.S. M. Montenegro, Ecotoxicological aspects related to the presence of pharmaceuticals in the aquatic environment, J. Hazard. Mater. 175 (2010) 45–95, https://doi.org/10.1016/j.jhazmat.2009.10.100.

[5] D. Deng, H. Yang, C. Liu, K. Zhao, J. Li, A. Deng, Ultrasensitive detection of diclofenac in water samples by a novel surface-enhanced Raman scattering (SERS)-based immunochromatographic assay using AgMBA@SiO2-ab as immunoprobe, Sens. Actuators B Chem. 283 (2019) 563–570, https://doi.org/10.1016/j.snb.2018.12.076.

[6] M. Mostafavi, M.R. Yaftian, F. Piri, H. Shayani-Jam, A new diclofenac molecularly imprinted electrochemical sensor based upon a polyaniline/reduced graphene oxide nano-composite, Biosens. Bioelectron. 122 (2018) 160–167, https://doi.org/10.1016/j.bios.2018.09.047.

[7] M. Scheurell, S. Franke, R.M. Shah, H. Hühnerfuss, Occurrence of diclofenac and its metabolites in surface water and effluent samples from Karachi, Pakistan, Chemosphere 77 (2009) 870–876, https://doi.org/10.1016/j.chemosphere.2009.07.066.

[8] X. Zhao, Y. Hou, H. Liu, Z. Qiang, J. Qu, Electro-oxidation of diclofenac at boron doped diamond: kinetics and mechanism, Electrochim. Acta 54 (2009) 4172–4179, https://doi.org/10.1016/J.ELECTACTA.2009.02.059.

[9] Y. Zhang, S.-U. Geißen, C. Gal, Carbamazepine and diclofenac: removal in wastewater treatment plants and occurrence in water bodies, Chemosphere 73 (2008) 1151–1161, https://doi.org/10.1016/j.chemosphere.2008.07.086.

[10] P. Paíga, M. Correia, M.J. Fernandes, A. Silva, M. Carvalho, J. Vieira, S. Jorge, J. G. Silva, C. Freire, C. Delerue-Matos, Assessment of 83 pharmaceuticals in WWTP influent and effluent samples by UHPLC-MS/MS: hourly variation, Sci. Total Environ. 648 (2019) 582–600, https://doi.org/10.1016/J.SCITOTENV.2018.08.129.

[11] V. Acuña, A. Ginebreda, J.R. Mor, M. Petrovic, S. Sabater, J. Sumpter, D. Barceló, Balancing the health benefits and environmental risks of pharmaceuticals: diclofenac as an example, Environ. Int. 85 (2015) 327–333, https://doi.org/10.1016/j.envint.2015.09.023.

[12] T. Reemtsma, S. Weiss, J. Mueller, M. Petrovic, S. González, D. Barcelo, F. Ventura, T.P. Knepper, Polar pollutants entry into the water cycle by municipal wastewater: a European perspective, Environ. Sci. Technol. 40 (2006) 5451–5458, https://doi.org/10.1021/es060908a.

[13] M. Huebner, E. Weber, R. Niessner, S. Boujday, D. Knopp, Rapid analysis of diclofenac in freshwater and wastewater by a monoclonal antibody-based highly sensitive ELISA, Anal. Bioanal. Chem. 407 (2015) 8873–8882, https://doi.org/10.1007/s00216-015-9048-9.

[14] L. Bouly, F. Courant, E. Bonnafé, J.-L. Carayon, J.-M. Malgouyres, C. Vignet, E. Gomez, F. Géret, H. Fenet, Long-term exposure to environmental diclofenac concentrations impairs growth and induces molecular changes in Lymnaea stagnalis freshwater snails, Chemosphere 291 (2022) 133065, https://doi.org/10.1016/j.chemosphere.2021.133065.

[15] J.M. Brozinski, M. Lahti, A. Meierjohann, A. Oikari, L. Kronberg, The anti-inflammatory drugs diclofenac, naproxen and ibuprofen are found in the bile of wild fish caught downstream of a wastewater treatment plant, Environ. Sci. Technol. 47 (2013) 342–348, https://doi.org/10.1021/ES303013J/SUPPL_FILE/ES303013J_SI_001.PDF.

[16] B. Hoeger, B. Köllner, D.R. Dietrich, B. Hitzfeld, Water-borne diclofenac affects kidney and gill integrity and selected immune parameters in brown trout (Salmo trutta f. fario), Aquat. Toxicol. 75 (2005) 53–64, https://doi.org/10.1016/J.AQUATOX.2005.07.006.

[17] J. Schwaiger, H. Ferling, U. Mallow, H. Wintermayr, R.D. Negele, Toxic effects of the non-steroidal anti-inflammatory drug diclofenac, Aquat. Toxicol. 68 (2004) 141–150, https://doi.org/10.1016/j.aquatox.2004.03.014.

[18] T. Heberer, Tracking persistent pharmaceutical residues from municipal sewage to drinking water, J. Hydrol. 266 (2002) 175–189, https://doi.org/10.1016/S0022-1694(02)00165-8.

[19] M. Česen, E. Heath, Disk-based solid phase extraction for the determination of diclofenac and steroidal estrogens E1, E2 and EE2 listed in the WFD watch list by GC–MS, Sci. Total Environ. 590–591 (2017) 832–837, https://doi.org/10.1016/j.scitotenv.2017.02.222.

[20] D. Löffler, T.A. Ternes, Determination of acidic pharmaceuticals, antibiotics and ivermectin in river sediment using liquid chromatography–tandem mass spectrometry, J. Chromatogr. A 1021 (2003) 133–144, https://doi.org/10.1016/j.chroma.2003.08.089.

[21] S.D. Jadhav, S.R. Butle, S.D. Patil, P.K. Jagtap, Validated stability indicating RP-HPLC method for simultaneous determination and in vitro dissolution studies of thiocolchicoside and diclofenac potassium from tablet dosage form, Arab. J. Chem. 8 (2015) 118–128, https://doi.org/10.1016/j.arabjc.2011.01.018.

[22] M. Petrović, M.D. Hernando, M.S. Díaz-Cruz, D. Barceló, Liquid chromatography–tandem mass spectrometry for the analysis of pharmaceutical residues in environmental samples: a review, J. Chromatogr. A 1067 (2005) 1–14, https://doi.org/10.1016/j.chroma.2004.10.110.

[23] J.D. Cahill, E.T. Furlong, M.R. Burkhardt, D. Kolpin, L.G. Anderson, Determination of pharmaceutical compounds in surface- and ground-water samples by solid-phase extraction and high-performance liquid chromatography–electrospray ionization mass spectrometry, J. Chromatogr. A 1041 (2004) 171–180, https://doi.org/10.1016/j.chroma.2004.04.005.

[24] R. Rosen, Mass spectrometry for monitoring micropollutants in water, Curr. Opin. Biotechnol. 18 (2007) 246–251, https://doi.org/10.1016/j.copbio.2007.03.005.

[25] A.A. Pebdani, A.M.H. Shabani, S. Dadfarnia, S. Khodadoust, Solid phase microextraction of diclofenac using molecularly imprinted polymer sorbent in hollow fiber combined with fiber optic-linear array spectrophotometry, Spectrochim. Acta. A. Mol. Biomol. Spectrosc. 147 (2015) 26–30, https://doi.org/10.1016/j.saa.2015.03.057.

[26] M.A. Castillo, L. Bruzzone, Indirect Fluorometric determination of diclofenac sodium, Anal. Sci. 22 (2006) 431–433, https://doi.org/10.2116/analsci.22.431.

[27] Theia'a N. Al-Sabha, Intisar A. Alhamoodi, Spectrofluorimetric determination of propranolol and diclofenac medicines using fluorescein dye, J. Anal. Chem. 78 (2023) S26–S34, https://doi.org/10.1134/S106193482403002X.

[28] M. Goodarzian, M.A. Khalilzade, F. Karimi, V. Kumar Gupta, M. Keyvanfard, H. Bagheri, M. Fouladgar, Square wave voltammetric determination of diclofenac in liquid phase using a novel ionic liquid multiwall carbon nanotubes paste electrode, J. Mol. Liq. 197 (2014) 114–119, https://doi.org/10.1016/j.molliq.2014.04.037.

[29] S.L.Z. Jiokeng, I.K. Tonle, A. Walcarius, Amino-attapulgite/mesoporous silica composite films generated by electro-assisted self-assembly for the voltammetric determination of diclofenac, Sens. Actuators B Chem. 287 (2019) 296–305, https://doi.org/10.1016/j.snb.2019.02.038.

[30] C.F. Poole, New trends in solid-phase extraction, TrAC, Trends Anal. Chem. 22 (2003) 362–373, https://doi.org/10.1016/S0165-9936(03)00605-8.

[31] F. Meier, B. Schott, D. Riedel, B. Mizaikoff, Computational and experimental study on the influence of the porogen on the selectivity of 4-nitrophenol molecularly

imprinted polymers, Anal. Chim. Acta 744 (2012) 68–74, https://doi.org/10.1016/j.aca.2012.07.020.
[32] M. Wang, J. Wang, Negative parental attribution and emotional dysregulation in Chinese early adolescents: harsh fathering and harsh mothering as potential mediators, Child Abuse Negl. 81 (2018) 12–20, https://doi.org/10.1016/j.chiabu.2018.04.008.
[33] M. Majd, M. Yazdanpanah, M.R. Bayatloo, S. Nojavan, Recent advances and applications of cyclodextrins in magnetic solid phase extraction, Talanta 229 (2021) 122296, https://doi.org/10.1016/j.talanta.2021.122296.
[34] Y. Zhang, S.N. Riduan, Functional porous organic polymers for heterogeneous catalysis, Chem. Soc. Rev. 41 (2012) 2083–2094, https://doi.org/10.1039/c1cs15227k.
[35] S. Fajal, S. Dutta, S.K. Ghosh, Porous organic polymers (POPs) for environmental remediation, Mater. Horiz. 10 (2023) 4083–4138, https://doi.org/10.1039/d3mh00672g.
[36] Z. Li, Y.-W. Yang, Creation and bioapplications of porous organic polymer materials, J. Mater. Chem. B 5 (2017) 9278–9290, https://doi.org/10.1039/c7tb02647a.
[37] N. Enjamuri, S. Sarkar, B.M. Reddy, J. Mondal, Design and catalytic application of functional porous organic polymers: opportunities and challenges, Chem. Rec. 19 (2019) 1782–1792, https://doi.org/10.1002/tcr.201800080.
[38] Y. Guo, J. Wang, L. Hao, Q. Wu, C. Wang, Z. Wang, Triazine-triphenylphosphine based porous organic polymer as sorbent for solid phase extraction of nitroimidazoles from honey and water, J. Chromatogr. A 1649 (2021) 462238, https://doi.org/10.1016/j.chroma.2021.462238.
[39] Z. Li, Y. Yang, Macrocycle-based porous organic polymers for separation, sensing, and catalysis, Adv. Mater. 34 (2022), https://doi.org/10.1002/adma.202107401.
[40] J. Szejtli, Introduction and general overview of Cyclodextrin chemistry, Chem. Rev. 98 (1998) 1743–1754, https://doi.org/10.1021/cr970022c.
[41] M.L. Bender, M. Komiyama, Cyclodextrin chemistry, springer Berlin Heidelberg, 1978, https://doi.org/10.1007/978-3-642-66842-5.
[42] W. Wang, A.E. Kaifer, Cucurbituril and Cyclodextrin complexes of dendrimers, Adv. Polym. Sci. 222 (2009) 205–235, https://doi.org/10.1007/12_2008_1.
[43] J.A. Arancibia, G.M. Escandar, Complexation study of diclofenac with b-cyclodextrin and spectrofluorimetric determination, Analyst 124 (1999) 1833–1838, https://doi.org/10.1039/A906719A.
[44] M. Bogdan, M.R. Caira, D. Bogdan, C. Morari, S.I. Fărcaş, Evidence of a bimodal binding between diclofenac-Na and β-cyclodextrin in solution, J. Incl. Phenom. Macrocycl. Chem. 49 (2004) 225–229, https://doi.org/10.1023/B:JIPH.0000048311.02653.23.
[45] R.L. Carrier, L.A. Miller, I. Ahmed, The utility of cyclodextrins for enhancing oral bioavailability, J. Control. Release 123 (2007) 78–99, https://doi.org/10.1016/j.jconrel.2007.07.018.
[46] D. Whittaker, L. Penkler, Diclofenac–β–cyclodextrin inclusion in solution, J. Inclusion Phenom. Macrocycl. Chem. 49 (2004) 225–229, https://doi.org/10.1023/B:JIPH.0000038560.50693.8c.
[47] S. Moon, A. Saboe, M.J. Smanski, Using design of experiments to guide genetic optimization of engineered metabolic pathways, J. Ind. Microbiol. Biotechnol. 51 (2024) kuae010, https://doi.org/10.1093/jimb/kuae010.
[48] N. Benyahia, N. Belkhouche, J.Å. Jönsson, A comparative study of experimental optimization and response surface methodology of bi(III) extraction by emulsion organophosphorus liquid membrane, J. Environ. Chem. Eng. 2 (2014) 1756–1766, https://doi.org/10.1016/j.jece.2014.07.003.
[49] M.A. Bezerra, R.E. Santelli, E.P. Oliveira, L.S. Villar, L.A. Escaleira, Response surface methodology (RSM) as a tool for optimization in analytical chemistry, Talanta 76 (2008) 965–977, https://doi.org/10.1016/j.talanta.2008.05.019.
[50] R. Wang, Z.-W. Lin, M.J. Klemes, M. Ateia, B. Trang, J. Wang, C. Ching, D. E. Helbling, W.R. Dichtel, A tunable porous β-Cyclodextrin polymer platform to understand and improve anionic PFAS removal, ACS Cent. Sci. 8 (2022) 663–669, https://doi.org/10.1021/acscentsci.2c00478.
[51] Y. Shi, Z. Zhang, L. Li, N. Cao, L. Zhang, C. Hou, W. Zhang, K. Zhang, Simultaneous and rapid removal of organic micropollutants, heavy metal ions, and cationic dyes from water by a porous Cyclodextrin polymer, ACS Appl. Mater. Interfaces 17 (2025) 59434–59443, https://doi.org/10.1021/acsami.5c16039.
[52] Z.-W. Lin, E.F. Shapiro, F.J. Barajas-Rodriguez, A. Gaisin, M. Ateia, J. Currie, D. E. Helbling, R. Gwinn, A.I. Packman, W.R. Dichtel, Trace organic contaminant removal from municipal wastewater by Styrenic β-Cyclodextrin polymers, Environ. Sci. Technol. 57 (2023) 19624–19636, https://doi.org/10.1021/acs.est.3c04233.
[53] S.L.C. Ferreira, R.E. Bruns, H.S. Ferreira, G.D. Matos, J.M. David, G.C. Brandão, E. G.P. Da Silva, L.A. Portugal, P.S. Dos Reis, A.S. Souza, W.N.L. Dos Santos, Box-Behnken design: an alternative for the optimization of analytical methods, Anal. Chim. Acta 597 (2007) 179–186, https://doi.org/10.1016/j.aca.2007.07.011.
[54] Y.-L. Li, Z.-X. Fang, J. You, Application of box-Behnken experimental design to optimize the extraction of insecticidal Cry1Ac from soil, J. Agric. Food Chem. 61 (2013) 1464–1470, https://doi.org/10.1021/jf304970g.
[55] N.A. Samah, M.-J. Sánchez-Martín, R.M. Sebastián, M. Valiente, M. López-Mesas, Molecularly imprinted polymer for the removal of diclofenac from water: synthesis and characterization, Sci. Total Environ. 631–632 (2018) 1534–1543, https://doi.org/10.1016/j.scitotenv.2018.03.087.
[56] A. Keutgen, S. Hotz, F. Shi, A.J.C. Kuehne, 3D-Stereolithographically printed mesoscopic microgels with precisely positioned supramolecular recognition motifs—soft building blocks for assembly and light triggered disassembly, Chem. Mater. 36 (2024) 1472–1481, https://doi.org/10.1021/acs.chemmater.3c02708.
[57] M.I. Slavkova, D.B. Momekova, B.D. Kostova, G.T. Momekov, P.D. Petrov, Novel dextran/β-cyclodextrin and dextran macroporous cryogels for topical delivery of curcumin in the treatment of cutaneous T-cell lymphoma, Bulg. Chem. Commun. 49 (2017) 792–799.
[58] E.E. Mitsika, C. Christophoridis, N. Kouinoglou, N. Lazaridis, C.K. Zacharis, K. Fytianos, Optimized photo-Fenton degradation of psychoactive pharmaceuticals alprazolam and diazepam using a chemometric approach—structure and toxicity of transformation products, J. Hazard. Mater. 403 (2021) 123819, https://doi.org/10.1016/J.JHAZMAT.2020.123819.
[59] V. Hosseinpour, M. Kazemeini, A. Mohammadrezaee, Optimisation of Ru-promoted Ir-catalysed methanol carbonylation utilising response surface methodology, Appl. Catal. Gen. 394 (2011) 166–175, https://doi.org/10.1016/j.apcata.2010.12.036.
[60] D. Allouss, Y. Essamlali, O. Amadine, A. Chakir, M. Zahouily, Response surface methodology for optimization of methylene blue adsorption onto carboxymethyl cellulose-based hydrogel beads: adsorption kinetics, isotherm, thermodynamics and reusability studies, RSC Adv. 9 (2019) 37858–37869, https://doi.org/10.1039/C9RA06450H.
[61] E. Kalydi, M. Malanga, T.T. Nielsen, R. Wimmer, S. Béni, Solving the puzzle of 2-hydroxypropyl β-cyclodextrin: detailed assignment of the substituent distribution by NMR spectroscopy, Carbohydr. Polym. 338 (2024) 122167, https://doi.org/10.1016/j.carbpol.2024.122167.
[62] S. Tang, L. Kong, J. Ou, Y. Liu, X. Li, H. Zou, Application of cross-linked β-cyclodextrin polymer for adsorption of aromatic amino acids, J. Mol. Recognit. 19 (2006) 39–48, https://doi.org/10.1002/jmr.756.
[63] J. Norooz Oliaee, M. Dehghany, A.R.W. McKellar, N. Moazzen-Ahmadi, High resolution infrared spectroscopy of carbon dioxide clusters up to (CO2)13, J. Chem. Phys. 135 (2011) 044315, https://doi.org/10.1063/1.3615543.
[64] A. Hebb, Synthesis of porous cross-linked polymer monoliths using 1,1,1,2-tetra-fluoroethane (R134a) as the porogen, Compos. Sci. Technol. 63 (2003) 2379–2387, https://doi.org/10.1016/s0266-3538(03)00271-9.
[65] A.A. Abdoh, M.B. Zughul, J. Eric, D. Davies, A.A. Badwan, Inclusion complexation of diclofenac with natural and modified cyclodextrins explored through phase solubility, 1H-NMR and molecular modeling studies, J. Incl. Phenom. Macrocycl. Chem. 57 (2007) 503–510, https://doi.org/10.1007/s10847-006-9241-8.
[66] F.P. Byrne, S. Jin, G. Paggiola, T.H.M. Petchey, J.H. Clark, T.J. Farmer, A.J. Hunt, C. Robert McElroy, J. Sherwood, Tools and techniques for solvent selection: green solvent selection guides, Sustain. Chem. Process. 4 (2016) 7, https://doi.org/10.1186/s40508-016-0051-z.
[67] M.L. Manca, M. Zaru, G. Ennas, D. Valenti, C. Sinico, G. Loy, A.M. Fadda, Diclofenac-β-cyclodextrin binary systems: physicochemical characterization and in vitro dissolution and diffusion studies, AAPS PharmSciTech 6 (2005) E464–E472, https://doi.org/10.1208/pt060358.
[68] K. Yetilmezsoy, S. Demirel, R.J. Vanderbei, Response surface modeling of Pb(II) removal from aqueous solution by *Pistacia vera* L.: box–behnken experimental design, J. Hazard. Mater. 171 (2009) 551–562, https://doi.org/10.1016/j.jhazmat.2009.06.035.
[69] Y.-P. Duan, C.-M. Dai, Y.-L. Zhang, Ling-Chen, selective trace enrichment of acidic pharmaceuticals in real water and sediment samples based on solid-phase extraction using multi-templates molecularly imprinted polymers, Anal. Chim. Acta 758 (2013) 93–100, https://doi.org/10.1016/j.aca.2012.11.010.
[70] A. Mpupa, M. Dinc, B. Mizaikoff, P.N. Nomngongo, Exploration of a molecularly imprinted polymer (MIPs) as an adsorbent for the enrichment of Trenbolone in water, Processes 9 (2021) 186, https://doi.org/10.3390/pr9020186.
[71] L.M. Madikizela, L. Chimuka, Determination of ibuprofen, naproxen and diclofenac in aqueous samples using a multi-template molecularly imprinted polymer as selective adsorbent for solid-phase extraction, J. Pharm. Biomed. Anal. 128 (2016) 210–215, https://doi.org/10.1016/j.jpba.2016.05.037.
[72] G. Castronuovo, M. Niccoli, Thermodynamics of inclusion complexes of natural and modified cyclodextrins with acetylsalicylic acid and ibuprofen in aqueous solution at 298K, Thermochim. Acta 557 (2013) 44–49, https://doi.org/10.1016/j.tca.2013.01.037.
[73] A. Aboel Dahab, D. El-Hag, Rapid analysis of NSAIDs binding to β-cyclodextrin using the simultaneous measurement of absorption and circular dichroism with a novel multi-cell low-volume device, Anal. Bioanal. Chem. 404 (2012) 1839–1850, https://doi.org/10.1007/s00216-012-6286-y.
[74] E. Bertaut, J.-F. Goossens, D. Landy, C. Danel, Binding constants determination of cyclodextrin inclusion complexes by affinity capillary electrophoresis. How to overcome the limitations induced by the UV-detector? J. Chromatogr. A 1623 (2020) 461209 https://doi.org/10.1016/j.chroma.2020.461209.
[75] S. Choudhury, K.F. Nelson, Improvement of oral bioavailability of carbamazepine by inclusion in 2-hydroxypropyl-β-cyclodextrin, Int. J. Pharm. (1992) 175–180, https://doi.org/10.1016/0378-5173(92)90146-S.
[76] T. Fukahori, M. Kondo, S. Nishikawa, Dynamic study of interaction between β-Cyclodextrin and aspirin by the ultrasonic relaxation method, J. Phys. Chem. B 110 (2006) 4487–4491, https://doi.org/10.1021/jp058205n.
[77] H. Zhang, H. Zhang, W. Jin, L. Ding, Determination of dissociation constants of Cyclodextrin—ligand inclusion complexes by electrospray ionization mass spectrometry, Eur. J. Mass Spectrom. 12 (2006) 291–299, https://doi.org/10.1255/ejms.818.
[78] S. Suenaga, H. Kataoka, K. Hasegawa, R. Koga, C. Tsunoda, W. Kuwashima, T. Tsuchida, S. Goto, How does the powder mixture of ibuprofen and caffeine attenuate the solubility of ibuprofen? Comparative study for the xanthine derivatives to recognize their intermolecular interactions using Fourier-transform infrared (FTIR) spectra, differential scanning calorimetry (DSC), and X-ray powder Diffractometry (XRPD), Mol. Pharm. 21 (2024) 4524–4540, https://doi.org/10.1021/acs.molpharmaceut.4c00429.

[79] E. Ramachandran, S. Ramukutty, Growth, morphology, spectral and thermal studies of gel grown diclofenac acid crystals, J. Cryst. Growth 389 (2014) 78–82, https://doi.org/10.1016/j.jcrysgro.2013.11.081.
[80] T. Iliescu, M. Baia, V. Miclăuș, A Raman spectroscopic study of the diclofenac sodium–β-cyclodextrin interaction, Eur. J. Pharm. Sci. 22 (2004) 487–495, https://doi.org/10.1016/j.ejps.2004.05.003.
[81] E. Bilensoy, O. Gürkaynak, M. Ertan, M. Şen, A.A. Hıncal, Development of nonsurfactant Cyclodextrin nanoparticles loaded with anticancer drug paclitaxel, J. Pharm. Sci. 97 (2008) 1519–1529, https://doi.org/10.1002/jps.21111.
[82] G. Varan, J.M. Benito, C.O. Mellet, E. Bilensoy, Development of polycationic amphiphilic cyclodextrin nanoparticles for anticancer drug delivery, Beilstein J. Nanotechnol. 8 (2017) 1457–1468, https://doi.org/10.3762/bjnano.8.145.
[83] M.A. Waqar, M. Zaman, H. Hameed, M. Jamshaid, A. Irfan, G.A. Shazly, A.C. Paiva-Santos, Y.A. Bin Jardan, Formulation, characterization, and evaluation of β-cyclodextrin functionalized Hypericin loaded nanocarriers, ACS Omega 8 (2023) 38191–38203, https://doi.org/10.1021/acsomega.3c04444.
[84] M. Khademi, W. Wang, W. Reitinger, D.P.J. Barz, Zeta potential of poly(methyl methacrylate) (PMMA) in contact with aqueous electrolyte–surfactant solutions, Langmuir 33 (2017) 10473–10482, https://doi.org/10.1021/acs.langmuir.7b02487.
[85] Z. Podgórniak, W. Musiał, M.J. Kulus, D. Łacny, A. Budnik, T. Urbaniak, Synthesis and characterization of water-soluble EDTA-crosslinked poly-β-Cyclodextrins serving as ion-complexing drug carriers, Materials 19 (2026) 207, https://doi.org/10.3390/ma19010207.